UNIVERSIDADE DE SÃO PAULO
ESCOLA DE ENGENHARIA DE SÃO CARLOS

Giovanna Siqueira Mayese

Sensitivity Analysis for Parameterization of Generic Wind Generator Models

São Carlos
2025

Giovanna Siqueira Mayese

Sensitivity Analysis for Parameterization of Generic Wind Generator Models

Final thesis for the graduation course of Electrical Engineering of the Universidade de São Paulo for the degree of Bachelor in Electrical Engineering.
Supervisor: Prof. Rodrigo Andrade Ramos

São Carlos
2025

Giovanna Siqueira Mayese

Sensitivity Analysis for Parameterization of Generic Wind Generator Models

This final thesis has been considered suitable for obtaining the Bachelor's Degree in Electrical Engineering and approved in its final form by the Electrical Engineering Graduate Course.

São Carlos, June 27, 2025.

Reviewing Board:

Prof. Rodrigo Andrade Ramos
Universidade de São Paulo

MSc. Nicolas Abreu Rocha Leite Netto
Centro de Pesquisas de Energia Elétrica

Carolina Gonçalves Santos
Operador Nacional do Sistema

Ficha catalográfica elaborada pela Biblioteca Prof. Dr. Sérgio Rodrigues Fontes da EESC/USP com os dados inseridos pelo(a) autor(a).

Siqueira Mayese, Giovanna
S111s Sensitivity Analysis for Parameterization of Generic Wind Generator Models / Giovanna Siqueira Mayese; orientador Rodrigo Andrade Ramos. São Carlos, 2025.

Monografia (Graduação em Engenharia Elétrica com ênfase em Sistemas de Energia e Automação) -- Escola de Engenharia de São Carlos da Universidade de São Paulo, 2025.

1. Sensitivity Analysis. 2. Generic Models. 3. Parameter Estimation. 4. Frequency Stability. 5. Wind Generation. 6. Renewable Energy Sources. I. Título.

Eduardo Graziosi Silva - CRB - 8/8907

FOLHA DE APROVAÇÃO

Nome: Giovanna Siqueira Mayese

Título: "Sensitivity Analysis for Parameterization of Generic Wind Generator Models"

Trabalho de Conclusão de Curso defendido e aprovado em 27/06/2025,

com NOTA 10,0 (DEZ, ZERO), pela Comissão Julgadora:

Prof. Associado Rodrigo Andrade Ramos - Orientador SEL/EESC/USP

Mestre Carolina Gonçalves Santos - ONS

Mestre Nícolas Abreu Rocha Leite Netto - CEPEL

Coordenador da CoC-Engenharia Elétrica - EESC/USP:
Professor Associado José Carlos de Melo Vieira Júnior

ACKNOWLEDGEMENTS

I would like to express my deep gratitude to the University of São Paulo, an institution that has provided me with countless opportunities to learn, develop my skills, and connect with the world.

I also want to thank Professor Rodrigo Andrade Ramos, not only for his guidance in this and other projects but also for his support, encouragement, and invaluable teachings throughout this journey.

A special thanks to Professor Tatiane Fernandes, who was present at various key moments in my academic development and always showed willingness to assist me along the way.

With love and appreciation, I am deeply grateful to my family, who have always stood by my side, supporting me in the pursuit of my dreams. To my mother, for all her unwavering support; to my father, the only (not for much longer...) engineer in the family; and to my grandparents, who have continuously inspired me.

Finally, but never less importantly, I want to express my gratitude to my classmates and friends: Esther, Mika, Luciano, Iure, Ricardo, and Samuel, with whom I shared years of learning, challenges, and joy along this remarkable journey.

Eu gostaria de expressar minha profunda gratidão à Universidade de São Paulo, instituição que me proporcionou inúmeras oportunidades de aprender, desenvolver minhas habilidades me conectar com o mundo.

Também quero agradecer ao Professor Rodrigo Andrade Ramos, não apenas por sua orientação neste e em outros trabalhos, mas também pelo apoio, incentivo e ensinamentos ao longo dessa jornada.

A Professora Tatiane Fernandes, que esteve presente em diversos momentos fundamentais para o meu aprendizado e sempre demonstrou disposição para me auxiliar ao longo do caminho.

Com muito amor e carinho, agradeço à minha família, que sempre esteve ao meu lado, me apoiando na realização dos meus sonhos. À minha mãe, por todo apoio; ao meu pai, o único (não por muito mais tempo...) engenheiro da família; e aos meus avós, que sempre me inspiraram.

Por fim, mas nunca menos importante, agradeço aos meus colegas de sala e meus amigos: Esther, Mika, Luciano, Iure, Ricardo e Samuel, que eu compartilhei anos dessa jornada de aprendizado, desafios e diversão.

ABSTRACT

The increasing penetration of converter-interfaced generators (CIGs) from renewable sources, such as wind and solar energy, presents new operational challenges for power systems, particularly in the Northeast (NE) subsystem of the Brazilian Interconnected Power System (in portuguese, *Sistema Interligado Nacional* - SIN) , which is expected to expand significantly over the next decade. Addressing issues such as reduced equivalent inertia and frequency stability in this region requires complex studies with high computational effort. To overcome these challenges, developing reduced-order models is essential for evaluating dynamic behavior in high CIG penetration systems. Due to non-disclosure agreements (NDAs) , manufacturer-specific models remain inaccessible, forcing system agents who do not have access to models from all manufacturers to rely on generic models as an alternative for representing the dynamic behavior of Wind Farms (WF). This study investigates the role of standardized models for frequency stability analysis in wind power systems, with an emphasis on the representation of the NE system using a reduced equivalent of the region. The primary objective of this study is to identify the most relevant parameters for estimation within these models. To validate the proposed methodology, the WT3 phase II generic wind turbine model was selected as a case study. The approach involves estimating the parameters of this model through an optimization process, beginning with a sensitivity analysis to determine the most significant parameters, followed by the application of the Differential Evolution (DE) algorithm for parameter estimation. While these models offer several advantages, including reduced computational cost, simplified implementation, and broader applicability across various wind farms, the findings indicate that refinements are necessary for them to effectively capture the transient dynamics of full scale models, particularly in relation to reactive power behavior.

Keywords: Sensitivity Analysis; Generic Models; Parameter Estimation; Frequency Stability; Wind Generation, Renewable Energy Sources.

RESUMO

O aumento da penetração de geradores conectados por conversores (*Converter-Interfaced Generators* - CIGs) provenientes de fontes renováveis, como energia eólica e solar, apresenta novos desafios operacionais para os sistemas de potência, especialmente no subsistema Nordeste (NE) do Sistema Interligado Nacional (SIN), que deverá se expandir significativamente na próxima década. Abordar questões como a redução da inércia equivalente e a estabilidade de frequência nessa região exige estudos complexos com alto esforço computacional. Para superar esses desafios, o desenvolvimento de modelos de ordem reduzida é essencial para avaliar o comportamento dinâmico em sistemas com alta penetração de CIGs. Devido a acordos de confidencialidade (*Non-Disclosure Agreements* - NDAs), os modelos específicos dos fabricantes permanecem inacessíveis, forçando os agentes do sistema que não têm acesso aos modelos de todos os fabricantes a recorrer a modelos genéricos como alternativa para representar o comportamento dinâmico de parques eólicos (*Wind Farms* - WF). Este estudo investiga o papel dos modelos padronizados na análise da estabilidade de frequência em sistemas eólicos, com ênfase na representação do sistema NE por meio de um equivalente reduzido da região. O principal objetivo deste estudo é identificar os parâmetros mais relevantes para estimativa dentro desses modelos. Para validar a metodologia proposta, foi selecionado como estudo de caso o modelo genérico de turbina eólica WT3 fase II. A abordagem envolve a estimativa dos parâmetros desse modelo por meio de um processo de otimização, iniciando com uma análise de sensibilidade para determinar os parâmetros mais significativos, seguida da aplicação do algoritmo de Evolução Diferencial (*Differential Evolution* - DE) para a estimativa dos parâmetros. Embora esses modelos ofereçam diversas vantagens, incluindo menor custo computacional, implementação simplificada e aplicabilidade mais ampla em diferentes parques eólicos, os resultados indicam que são necessários refinamentos para que possam capturar de forma eficaz as dinâmicas transitórias dos modelos em escala completa, especialmente em relação ao comportamento da potência reativa.

Palavras-chave: Análise de sensibilidade; modelos genéricos; estimativa de parâmetros; esta-bilidade de frequência; geração eólica, fontes de energia renováveis.

LIST OF FIGURES

LIST OF ABBREVIATIONS AND ACRONYMS

Brazilian Interconnected Power System SIN

Brazilian National System Operator ONS

Converter-Interfaced Generation CIG

Differential Evolution DE

Doubly-Fed Induction Generators DFIG

Electrical Power System EPS

Energy Expansion Plan EEP

Hydroelectric Power Plants HPPs

International Electrotechnical Commission IEC

Laboratory of Analysis and Control of Electrical Power Systems LACSEP

Mean Square Error MSE

Power System Stabilizers PSS

Renewable Energy Sources RES

Rio Grande do Norte RN

Thermal Power Plants TPPs

Trajectory Sensitivity Analysis TSA

Trajectory Sensitivity Functions TSF

University of São Paulo USP

Western Electricity Coordinating Council WECC

Wind Farms WFs

CONTENTS

1 INTRODUCTION

The Electrical Power System (EPS) is a set of components whose function is to generate, transmit, and distribute electrical energy from power plants to consumer loads, ensuring that the voltage and frequency levels remain within acceptable ranges. However, voltage and frequency stability is a complex phenomenon and difficult to analyze in power systems, especially since, in the 21st century, EPSs have been forced to operate close to their stability limits (KUNDUR, 1994).

In Brazil, the production and transmission of electrical energy is characterized by the Brazilian Interconnected Power System (SIN), which can be classified as a large-scale hydro-thermal-wind system, with a predominance of hydroelectric plants interconnecting the South, Southeast, Midwest, North, and Northeast regions through a network of transmission lines. This operation involves complex simulation models coordinated and controlled by the Brazilian National System Operator (in portuguese, *Operador Nacional do Sistema* - ONS), which, in turn, is supervised and regulated by the National Electric Energy Agency (in portuguese, *Agência Nacional de Energia Elétrica* - ANEEL).

In recent years, there has been a significant increase in the share of Converter-Interfaced Generation (CIG) from Renewable Energy Sources (RES) in several countries, including Brazil. This expansion is likely to intensify in the coming decades, driven by global decarbonization policies and technological advances in the areas of wind and solar photovoltaic generation (HURTADO et al., 2024). Despite the benefits of this energy transition, the high penetration of CIG, coupled with the proportional reduction in conventional synchronous generation, poses new challenges for the operation of EPS. For example, the high penetration of these generators reduces the equivalent inertia of the system, affecting the inertial response and frequency control, which can lead to stability problems such as sudden frequency drops and the activation of special protection schemes (ALAM et al., 2023).

Today in Brazil, the penetration of CIG based on RES has a high prevalence in NE subsystem, with particularly wind and solar energy. In 2020, the SIN exceeded 16 GW of installed wind power generation capacity, spread across 751 wind farms with a total of 8.800 wind turbines (ABEEÓLICA, 2022). Nearly 90% of this capacity is concentrated at the NE subsystem of the SIN. According to the 2032 Energy Expansion Plan (EEP) (EPE, 2022), the next decade is expected to witness a 10 GW increase in installed CIG-based renewable generation capacity (including not only wind but also solar generation) in the north/northeast region of Brazil. On the other hand, the number of hydroelectric and fossil fuel power plants in the NE subsystem (corresponding currently to less than 50% of this subsystem's total power generation capacity) is projected to remain unchanged (EPE, 2022). Consequently, the NE subsystem may increasingly rely on other subsystems of the SIN, making the stability and resilience of the interconnected system a critical concern.

This growing dependence on inter-subsystem energy exchange further underscores the importance of precise dynamic response, particularly during grid disturbances. During the blackout in August 15^{th}, 2023, proper dynamic representation was crucial to identify the cause of the problem, isolate affected areas, and efficiently restore the power supply. Events like this highlight the need for a well-parameterized system with accurate models to mitigate impacts and improve SIN resilience.

According to the Disturbance Analysis Report (in portuguese, *Relatório de Análise de Perturbação* - RAP), published by Brazilian National System Operator (ONS) after this incident, the disturbance analysis revealed that the performance of field controls in wind and solar power plants — particularly regarding their capability to support dynamic reactive power — was far below the simulation models provided by agents and represented in the official transient electromechanical database. It was also found that the discrepancy between field performance and simulations did not allow for the identification of risks associated with the pre-disturbance operational scenario, which led to cascading outages after the opening of the 500 kV Fortaleza II - Quixadá Transmission Line, located in the NE region. Therefore, one of ONS's guidelines is to develop a validation guide for simulation models of wind and photovoltaic power plants (ONS, 2023).

Parameterization of active power system models involves adjusting and defining specific parameters in simulation models that represent electrical distribution systems, particularly those that include distributed generation, energy storage, and automated control devices. The goal is to ensure that these models accurately reflect the real behavior of systems under various operating conditions.

However, in the Brazilian scenario, manufacturer-specific models are often protected by NDAs, restricting access to their detailed specifications. Consequently, even when an entity seeks to simulate a particular model, it may not be openly available. As a result, system operators and researchers, who do not have access to models from all manufacturers, must rely on dynamic behavioral representations of other Wind Farms (WFs) and power plants to ensure comprehensive analyses.

The increasing penetration of wind energy in modern power systems has further accentuated the need for standardized models in stability studies. Among these, the WT3 generic wind model has gained prominence for its ability to represent wind turbines employing Doubly-Fed Induction Generators (DFIG) (EIRÓ, 2018). Widely used in power system simulations, this model facilitates assessments of Wind Farms dynamics under various grid conditions, helping to bridge gaps created by proprietary model restrictions and advancing the understanding of renewable energy integration.

Considering the increasing need for the Brazilian power system to maintain a resilient grid through the validation of simulation models for wind power plants, this final thesis investigates the use of generic models made available by WECC to represent the dynamic behavior of WFs from various manufacturers in the state of Rio Grande

do Norte, within the Northeast subsystem. To parameterize the dynamic models of WF aggregates, this work proposes a methodology based on the solution of an optimization problem. The methodology involves simulations with the original WF models provided by the agents/manufacturers, to extract signals from the terminal busbars of the WF of interest (target generators), combined with simulations of the reduced NE system, in which the WF aggregates are represented by the generic dynamic models. To reduce computational cost, the relevant parameters of the generic models of the target generators are identified using Trajectory Sensitivity Analysis (TSA), followed by the application of Differential Evolution (DE) algorithm for parameter estimation.

This final thesis is structured as follows: Section 2 presents the theoretical framework of the reduced equivalent of the NE system, as well as the WECC model general blocks; Section 3 details the proposed methodology for the model sensitivity analysis and parameterization; Section 4 presents a case study; and finally, Section 5 discusses the conclusions and future perspectives of this study.

1.1 GENERAL OBJECTIVES

The main objective of this study is to develop and apply a trajectory sensitivity methodology to help tune the parameters in a generic WT3 wind generator model in order to contribute to the development of reduced-order models for the study of interconnected power systems in the parameterization of wind generation.

The relevance of this improvement becomes clear in the light of past critical events, such as the one that took place on August 15^{th}, 2023, which highlighted the need for a more accurate representation of these sectors in order to improve the system's resilience and ability to respond in adverse situations. In this way, the effective implementation of the proposed sensitivity analysis and parameterization aims not only to optimize operations, but also can to reduce risks and improve the security and stability of the SIN in challenging scenarios.

1.2 SPECIFIC OBJECTIVES

In order to achieve the general objective mentioned above, the specific objectives are as follows:

- Perform dynamic simulations on the equivalent model based on the NE region;
- Identify the parameters that have the greatest influence on the response of the WT3 model wind generators by applying TSA;
- Expose a parametrization using DE algorithm and tune the more sensitive parameters.

2 THEORETICAL FRAMEWORK

2.1 TEST SYSTEM BASED ON THE NE ELECTRICAL POWER SUBSYSTEM

The NE subsystem of the SIN is characterized by a high penetration of CIG from RES, particularly wind and solar power. This high level of wind and solar generation makes the NE subsystem an ideal test bed for studying CIG-based RES, inertia reduction, and primary frequency control at a large scale. Consequently, the NE subsystem is likely to become increasingly dependent on other SIN subsystems for frequency support, particularly during contingency events. For this thesis, the test system used to represent the NE subsystem is based on the Technical Report (KUIAVA et al., 2025), developed by the research group of Laboratory of Analysis and Control of Electrical Power Systems (LACSEP) at University of São Paulo (USP).

The proposed test system comprises 224 buses, 422 AC transmission lines and transformers, with voltage levels of 500 kV (66 buses) and 230 kV (60 buses). The system equivalent loads are coupled to 53 buses. Furthermore, the equivalent system contains 60 Wind Farms (WFs), 19 Hydroelectric Power Plants (HPPs), and 18 Thermal Power Plants (TPPs). The total power generation capacity is approximately 22,400 MW, where the WFs, HPPs, and TPPs correspond to 11,200 MW (50% of the total), 5,800 MW (25.8% of the total) and 5,400 MW (24.2% of the total), respectively. The load of the NE system for the operating point adopted in the report is 13,900 MW. This mix of synchronous and asynchronous generation represents the main feature of this system, as it allows the analysis of the main issues that may arise in power systems in the transition to a high penetration of renewable sources connected to the grid by inverters. Conversely, when the total power generated exceeds the consumption or export capacity, it can lead to overvoltage conditions, frequency instability, generator tripping, and even potential damage to equipment. Therefore, accurately modeling such scenarios is critical for assessing system reliability and ensuring stable operation under varying conditions.

Normaly, the NE exchange power with the North and Southeast subsystems. However, in the report, the NE subsystem was considered as a control area of the SIN and, therefore, it is responsible for handling its own power imbalances, so the power exchanges with the other subsystems are constant. This is the main difference between our proposed system and the actual operation of the NE subsystem of the SIN and does not reflect the actual way this subsystem is operated in practice by the ONS. However, the main value of our proposed test system is the fact that it allows the study of possible local solutions for frequency stability problems related to events occurring internally in this subsystem, as well as other problems related to the high penetration of wind generation.

2.1.1 System Reduction

In the report (KUIAVA et al., 2025), the simplified model of the NE subsystem was developed by first extracting the complete NE subsystem from the SIN model. To do this, internal boundary buses in the NE subsystem were identified. Each one was considered to be an equivalent generator (PV-type bus) exporting or importing an active power value equivalent to the power exchanged between the internal (NE) and external subsystems for the nominal case.

The proposed test system based on the NE electrical power subsystem was then obtained from the application of the extended Ward equivalent method in the SIN, available in ANAREDE, to extract the complete NE electrical power subsystem. After that, the following reduction steps and simplifications were applied to the complete model of the NE subsystem:

1. All the transmission and sub-transmission buses in the NE subsystem with voltage levels below 230 kV (for example, 138 kV, 69 kV, and so on) were eliminated from the application of the extended Ward equivalent method;
2. All the WFs connected to the same sub-transmission bus (at 34.5 kV) were aggregated into an equivalent WF. The equivalent WFs with a power capacity below 100 MW were eliminated from applying the extended Ward equivalent method, which means that some buses have a negative active load. Hence, each of the 61 WFs of the proposed test system represents, in fact, an aggregation of WFs connected in the same sub-transmission bus, providing more than 100 MW of active power to the grid;
3. All the HPPs and TPPs with power generation capacity below 30 MW were eliminated from the application of the extended Ward equivalent method;
4. All the buses of transmission and sub-transmission lines with radial configuration were eliminated from the application of the extended Ward equivalent method.

The one-line diagram of the proposed test system is shown in Figure 1. In this diagram, the WFs, HPPs, and TPPs are identified by the letters ‘W’, ‘H’, and ‘T’, respectively. The equivalent generators representing the external subsystems are represented by ‘E’. The original numbering and the names of the buses (from the SIN) were preserved in this proposed system. About 40% of the total lines are original ones from the SIN, while the remaining are fictitious lines (or transformers) that originated from the application of the extended Ward equivalent method (KUIAVA et al., 2025).

Figure 1 – The one-line diagram of the proposed test system based on the NE subsystem of the SIN.

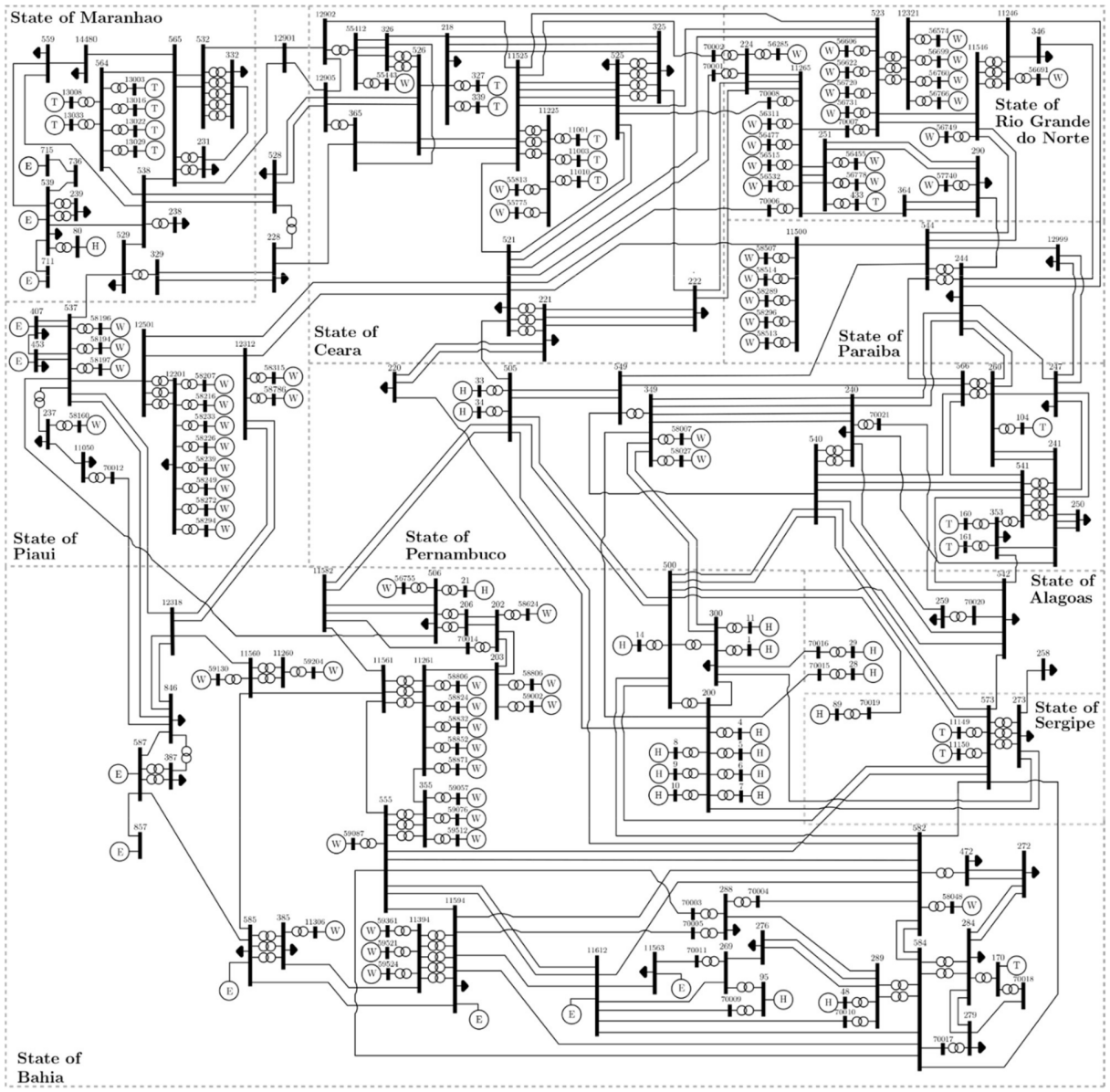

Source: (KUIAVA et al., 2025)

The HPPs and TPPs are represented by salient pole and round rotor synchronous machines, respectively. The salient pole units are modeled by a 5th-order dynamic model. Similarly, the generator model to represent the round rotor units is a 6th-order dynamic model. In both cases, the saturation effects were represented by exponential functions. All the HPPs and TPPs are equipped with an excitation system represented by the IEEE-type ST2A model. This is another feature of the system that does not exactly reproduce the equipment models of the actual NE subsystem of the SIN. However, the choice of simple standard models for controllers was made to facilitate the reproducibility of the test system. In addition, the HPPs and TPPs are equipped with Power System Stabilizers

(PSS), governor-turbine and speed regulation systems. Further detailed information on the representation is given in the report (KUIAVA et al., 2025).

Regarding WFs, represented by the letter 'W' in Figure 1, it is important to note that each WF corresponds to an aggregate of multiple WFs, modeled as a single WF providing 100 MW or more of active power to the grid. Therefore, since the parameterization process is conducted for each equivalent WF representing a wind farm aggregate, the abbreviation aWF will be adopted.

In the base case, regarding power injection from aWFs, the state of Rio Grande do Norte (RN) contributes the highest amount of active power in this operating scenario, reaching 3.9 GW. Consequently, this study focuses on the parameterization of generic models for aWF in this region.

For the aWF, in the simulations presented in this final thesis with an emphasis on RN, the 18 WF clusters in this region are represented using the WT3 WECC generic wind turbine dynamic stability model (phase II) (ESIG, 2025), while the remaining ones are modeled as constant current injections into the grid(KUIAVA et al., 2025). The details of the WT3 model are presented in the following section.

2.2 GENERIC WIND MODEL WT3

The WT3 model is designed to simulate the performance of wind turbines with Doubly-Fed Induction Generators (DFIG) technology, where the rotor is connected to the grid via an AC/DC/AC power converter (EIRÓ, 2018). This configuration allows for independent control of active and reactive power, enhancing the stability and efficiency of wind energy integration.

Different organizations have developed variations of the WT3 model to meet specific analytical needs. The International Electrotechnical Commission (IEC) and the Western Electricity Coordinating Council (WECC) have proposed different methodologies for modeling Type 3 wind turbines. While the WECC approach prioritizes simplicity and computational efficiency, the IEC model aims for higher fidelity by closely matching real turbine measurements (LORENZO-BONACHE et al., 2019).

The WT3 model is implemented on various simulation platforms, including Siemens PTI – PSSE and GE – PSLF, making it a versatile tool for power system operators. However, certain simplifications, such as the exclusion of flux dynamics, may limit its accuracy in extreme transient conditions.

The general structure of the second generation type 3 WTG model is illustrated in the block diagram in Figure 2.

Figure 2 – Type 3 WTG model Overall Structure.

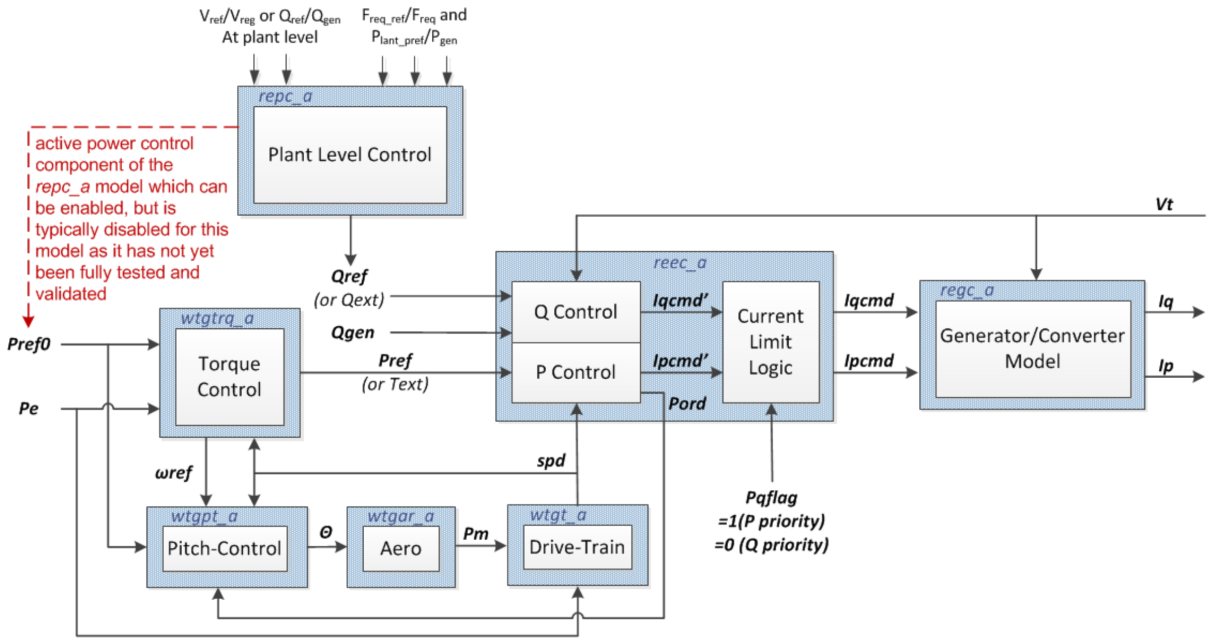

Source: (ESIG, 2025)

Each of the model control blocks are futher detalied bellow, Figure 3 to 9 shows the parameters related to the block. In total, the WT3 Phase II model has 76 parameters, and each typical value is detailed in the Apendix A of this study.

1. **Plant-Level Control Model (repc_a)** – which has inputs of either voltage reference (Vref) and measured/regulated voltage (Vreg) at the plant level, or reactive power reference (Qref) and measured (Qgen) at the plant level. The output of the repc_a model is a reactive power command that connects to Qref on the reec_a model.

Figure 3 – Plant-Level Control Model (repc_a).

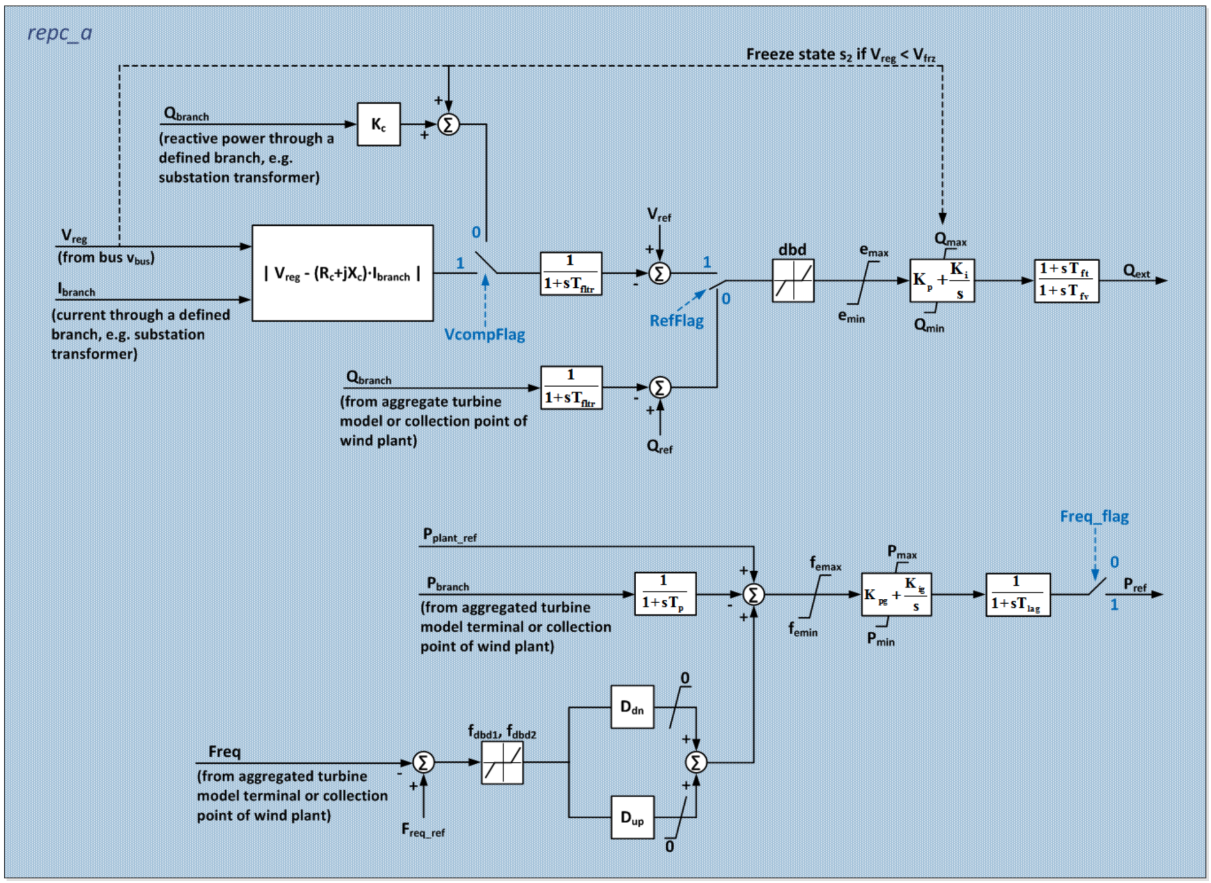

Source: (ESIG, 2025)

2. **Renewable Energy Electric Control Model (reec_a)** – which has inputs of real power reference (Pref) that can be externally controlled, reactive power reference (Qref) that can be externally controlled and feedback of the reactive power generated (Qgen). The outputs of this model are the real (Ipcmd) and reactive (Iqcmd) current command;

Figure 4 – Renewable Energy Electric Control Model (reec_a).

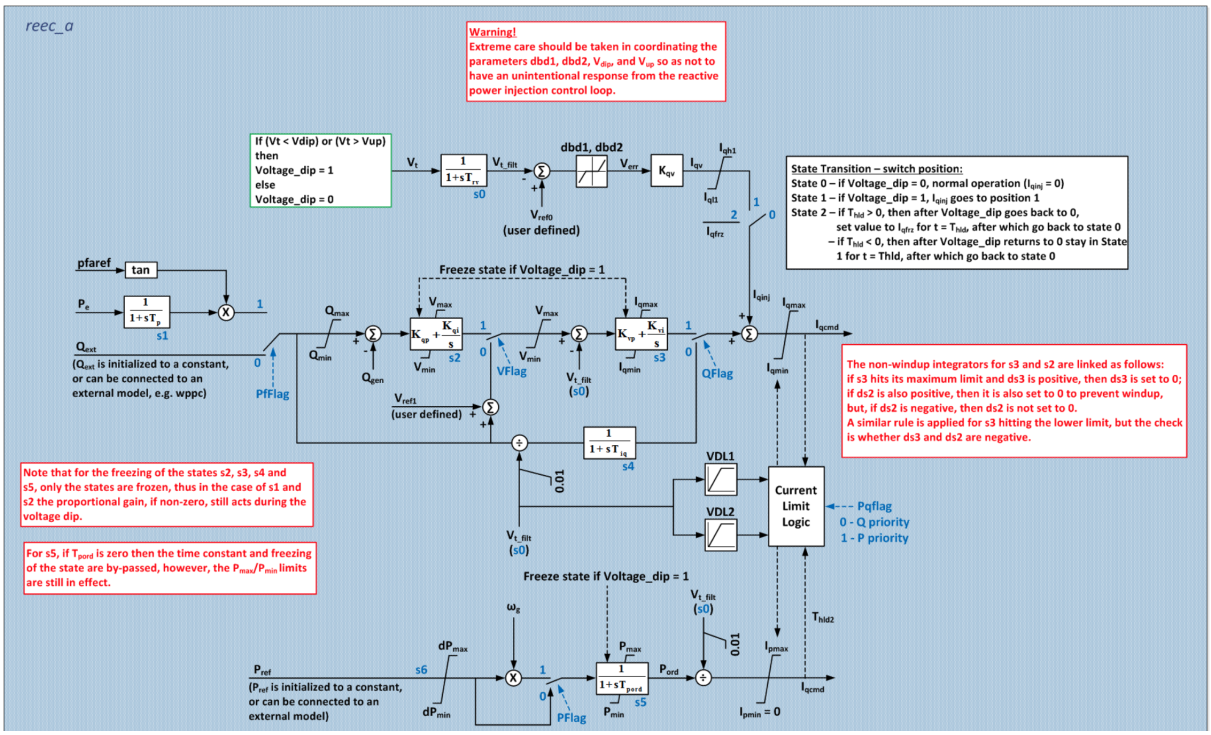

Source: (ESIG, 2025)

3. **Torque-Controller Model (wtgtrq_a)** – Manages the torque applied to the generator, ensuring stable operation and efficient energy conversion;

Figure 5 – Torque-Controller Model (wtgtrq_a).

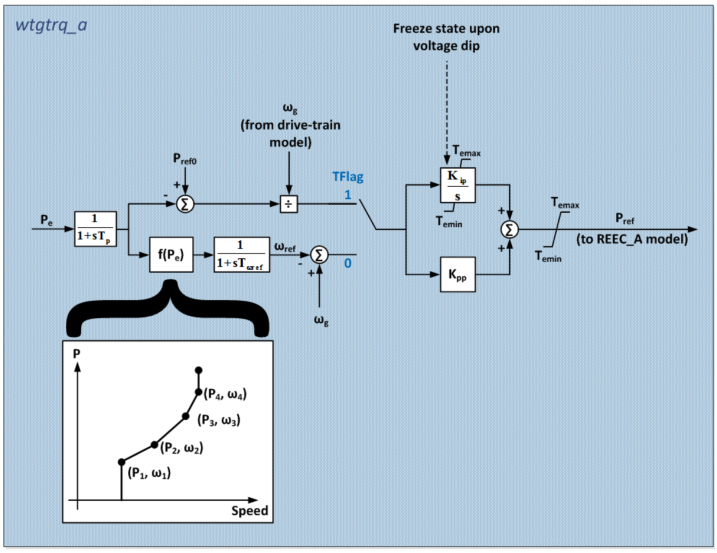

Source: (ESIG, 2025)

4. **Pitch-Controller Model (wtgpt_a)** – Regulates the pitch angle of the turbine blades to optimize power generation and protect the system from excessive wind speed;

Figure 6 – Pitch-Controller Model (wtgpt_a).

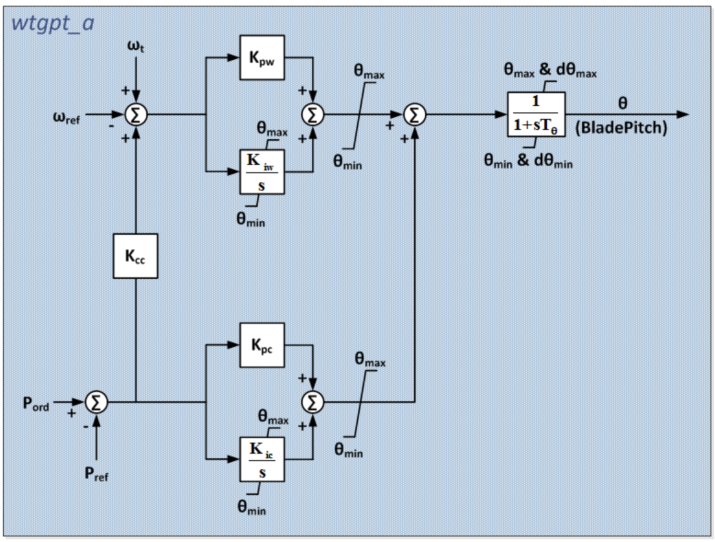

Source: (ESIG, 2025)

5. **Linear Aero-Dynamic Model (wtgar_a)** – Simulates the aerodynamic behavior of the wind turbine blades, determining the power extracted from the wind based on turbine characteristics;

Figure 7 – Linear Aero-Dynamic Model (wtgar_a).

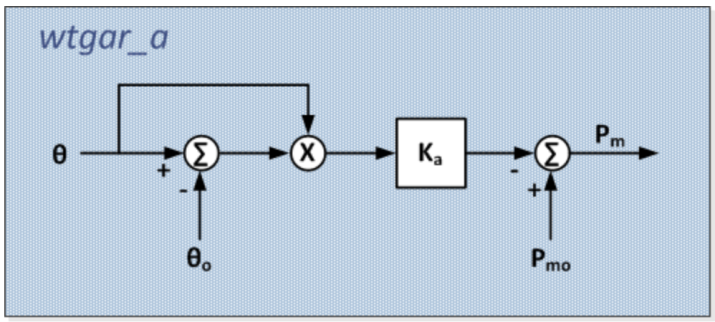

Source: (ESIG, 2025)

6. **Emulation of the Wind Turbine Generator Drive-Train (wtgt_a)** – Simulates drive-train oscillations. The output of this model is speed (spd). In this case speed is assumed to be a vector $spd = [\omega t\, \omega g]$, where ωt is the turbine speed and ωg the generator speed. It has been observed that, in this block diagram, the

model of the asynchronous prime mover machine is a simplified representation of the electromechanical dynamics. There are no equations related to the electrical fields of either the stator or the rotor. Consequently, in the event of a fault, the model is unable to represent the magnetic field discharge of the stator;

Figure 8 – Emulation of the Wind Turbine Generator Drive-Train (wtgt_a).

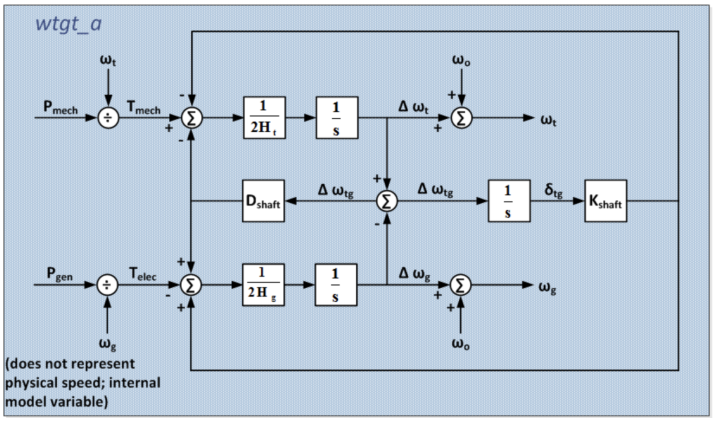

Source: (ESIG, 2025)

7. **Renewable Energy Generator/Converter Model (regc_a)** – This component models the renewable energy generator and converter, handling real (Ipcmd) and reactive (Iqcmd) current commands and injecting real (Ip) and reactive (Iq) current into the grid;

Figure 9 – Renewable Energy Generator/Converter Model (regc_a).

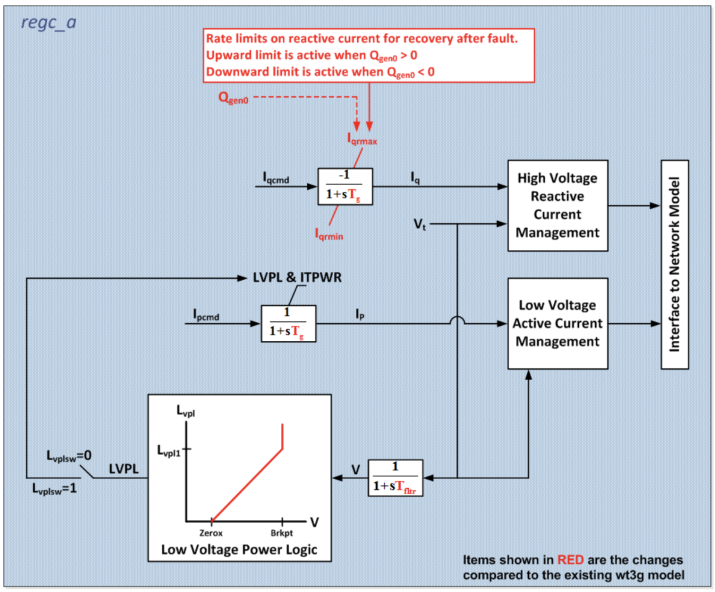

Source: (ESIG, 2025)

3 METHODOLOGY

The first step involves implementing the dynamic RMS test system for the system of interest, specifically by integrating the equivalent model files and the WT3 turbine model within the software ANATEM. In ANATEM, the WT3 model functions as a generic controlled source, with its behavior governed by the parameters of the generic WT3 model.

Subsequently, to perform the disturbance simulations, it is necessary to modify each of the 76 parameters in every analyzed bus and create a separate file for each system simulation based on the variation of a specific parameter. In other words, for each bus analyzed, 77 files had to be generated, one containing reference values and the others, each with only one parameter varied by 1%. To organize and automate this process, interface mechanisms were implemented between the software MATLAB and ANATEM, ensuring greater efficiency and practicality.

3.1 PARAMETER SENSITIVITY ANALYSIS

The results of these simulations are then used to calculate the trajectory sensitivity of each parameter of that busbar in relation to the system disturbance. Trajectory Sensitivity Functions (TSF) quantify the variation of the solution of differential equations concerning changes in their parameters (RAMOS et al., 2022). In model calibration, the most sensitive parameters are generally the most relevant, as they significantly influence the model's response, allowing its outputs to align with real measurements. Conversely, parameters with low sensitivity have negligible impact and are typically assigned standard values during the parameterization process (WANG et al., 2023).

The TSF for the k-th sample of the output signal $y_j(k)$ with respect to the i-th parameter θ_i can be approximated as:

$$TSF_k^{y_j} = \left| \frac{\partial y(\theta_i, k)/y_0}{\partial \theta_i/\theta_{i0}} \right| \approx \left| \frac{[y(\theta_i + \theta_{i,k}) - y(\theta_{i,k})]/y_0}{\Delta\theta_i/\theta_{i0}} \right| \tag{1}$$

where k refers to the k-th sample of the output signal, the subscript 0 indicates the steady-state (or reference) value, and $\Delta\theta_i$ represents a small perturbation in the parameter θ_i.

Based on the TSF values obtained for each sample, a sensitivity index ($E_{\theta_i} y_j$) is calculated for the parameter θ_i related to the output y_j, considering a window of N_w samples (GERALDI et al., 2020):

$$E_{\theta_i}^{y_j} = \sum_{k=1}^{N_w} (TSF_k^{y_j})^2 \tag{2}$$

For each aWP in the RN state in Figure 1 to which the generic WT3 model from WECC was applied, sensitivity analysis is performed on the frequency (F), active power

(P) and reactive power (Q) response of the model concerning each of its respective block parameters. Parameters with a high sensitivity index will be considered for estimation, while typical values specified in (ESIG, 2025), as detailed in (KUIAVA et al., 2025) and in the Apendix A of this work, will be adopted for the others parameters.

3.2 PARAMETER ESTIMATION

To estimate the parameters of the generic wind models, this study employs the Differential Evolution (DE) algorithm, a population-based stochastic optimization. DE is particularly effective for solving complex, nonlinear, and multi-modal optimization problems, making it well-suited for parameter estimation in dynamic energy systems.

In the parameterization process, as illustrated in the following Figure 10, it is essential to compare the response of the adjusted model with a reference response obtained under the same disturbance conditions. The optimization method then aims to minimize the error between these responses. With this objective in mind, the so-called reference system is defined based on the manufacturers' representations available in the SIN simulation files, according to the ONS database (ONS, 2024).

Figure 10 – Parametrization representation

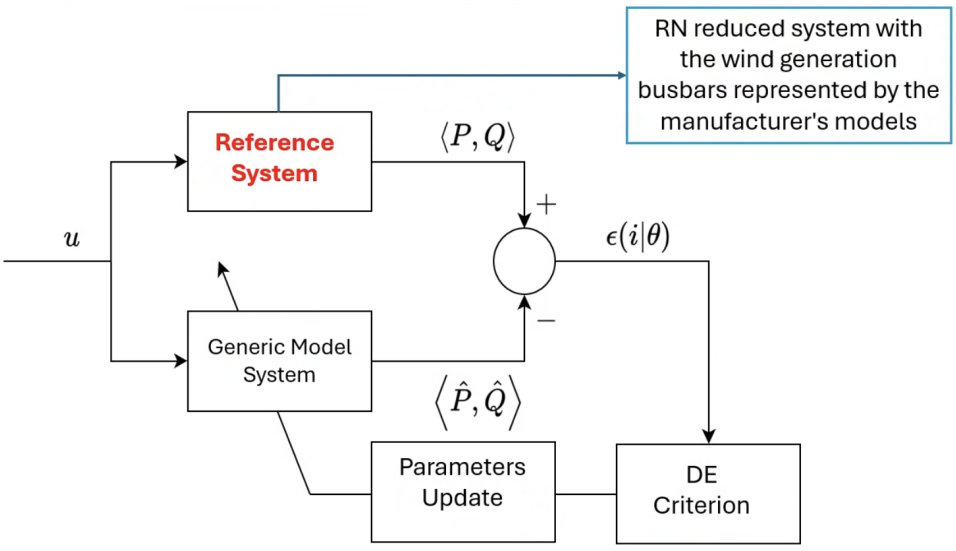

Source: Author

Initially, the WFs in the SIN corresponding to each aWF represented in the test system were identified, along with their respective dynamic models, which are provided by the manufacturers. In cases where multiple manufacturer's models were associated with the same aWF, the one with the highest installed capacity was adopted. The reference system was then generated from simulations of the reduced test system, replacing the generic models with the original manufacturer models, specifically in the studied region.

It is worth mentioning that the SIN database is currently undergoing an update process led by the ONS, which has requested agents/manufacturers to adjust the dynamic models of their WFs. This initiative was motivated by the conclusions of the disturbance analysis report regarding the event that occurred on August 15^{th}, 2023 (ONS, 2023).

The selected parameters are estimated based on sampled data from the reference system after the occurrence of a disturbance, such as a temporary short circuit. Then, the DE algorithm is applied and works by evolving a population of candidate solutions through three main operations: mutation, crossover, and selection. For each individual in the population, a mutant vector is generated by adding the weighted difference between two randomly selected individuals to a third one. This mutant vector is then combined with the original individual through crossover to produce a trial vector. If the trial vector yields a better objective function value, it replaces the original in the next generation. The algorithm is controlled by the key parameters: population size (N_p), mutation factor (F_s) and crossover rate (C_r)

As in other optimization methods, the DE algorithm aims to minimize the error between the reference system output and the test system outputs for a target generator, as defined by the objective function Mean Square Error (MSE) in Equation (3). In this work, the objective function is defined as a composite error metric based on both active power (P) and reactive power (Q) signals. This choice is motivated by the fact that both P and Q are directly influenced by the dynamic behavior of wind generators and their control systems. In particular, active power fluctuations are closely related to frequency stability, while reactive power dynamics affects voltage support and system damping. By incorporating both signals into the objective function, it is expected that that the resulting model accurately captures the system's response under realistic operating conditions, which is essential for frequency stability studies.

$$\min_{\theta} \epsilon(\theta) = \min_{\theta} \left[\frac{1}{N_w} \sum_{k=1}^{N_w} (P_k - \hat{P}_k(\theta))^2 \right] + \min_{\theta} \left[\frac{1}{N_w} \sum_{k=1}^{N_w} (Q_k - \hat{Q}_k(\theta))^2 \right] \tag{3}$$

subject to:

$$\theta_{\max} \leq \theta \leq \theta_{\min}$$

where P_k and Q_k correspond to the measured samples of active and reactive power in the reference system at the target generator's terminal bus. Meanwhile, $\hat{P}_k(\theta)$ and $\hat{Q}_k(\theta)$ represent the active and reactive power signals obtained at the terminal bus of the target generator in the test system for a given parameter vector θ. The limits $\theta_{\max}$ and $\theta_{\min}$ define the search space of the algorithm, which is established based on the typical physical values of each parameter in the generic WT3 model from WECC. Further details on the DE algorithm can be found in (LAMPINEN, 2005).

4 RESULTS

In order to investigate the capability of the generic WT3 Phase II WECC models in representing the aWFs of the test system, simulations were conducted using the ANATEM software. In the reference system, the aWFs located in the state of RN are represented by the manufacturers' models, while the others are modeled as constant current injections into the grid.

To stimulate the system response, a sudden outage of the TPP Porto Sergipe (state of Paraíba) connected to bus 11150 at $t = 0.5s$ was considered as the perturbation for the base case, based on the report (KUIAVA et al., 2025) Case 1.

4.1 PARAMETER SENSITIVITY ANALYSIS

From this event, the TSF for each parameter of the generic WT3 Phase II model connected to the respective bus was calculated for a 1% perturbation ($\Delta\theta_i$), with an integration step of $1ms$, within a response window of $5.0s$. Sensitivity indices were computed for the 76 model parameters.

4.1.1 RN Subsystem

First, for each aWP in the RN state in Figure 1, to which the generic WT3 model from WECC was applied, sensitivity analysis was performed on the Voltage (V), Frequency (F), Active Power (P) and Reactive Power (Q) response of the model regarding each of its respective block parameters. The busbars numbers, and their respective injected power, in the RN reduced subsystem where the generic WT3 model from WECC was applied are represented in Table 1 as follows:

Table 1 – RN reduced system busbars with WT3 model implemented and their respective power.

Busbar	**Active Power (MW)**
56477	528
56532	473
56515	444
56749	327
56691	279
56311	277
56760	176
56720	147

The Tables in Appendix B show the sensitivity index results related to the four output signals for a time window $T = 0.500$s to 5.0s. In each column, values in deeper red shades correspond to the highest sensitivity indices.

4.1.2 Case Study

To demonstrate the applicability of the method, the following results are presented for the aWP connected to bus 56532 in RN, which injects 473 MW of power in the base case. Initially, a wider time window was adopted to help better understand the sensitivity throughout the responses, but the time window must be adapted to the signal aimed at the analysis. This concept can be better illustrated with the following representation of the sensitivities curves of the signals in Figure 11:

Figure 11 – The images represent the (a) Active power, (b) Reactive power, (c) Frequency, (d) Voltage, sensitivity curves outputs of the TSF of bus 56532.

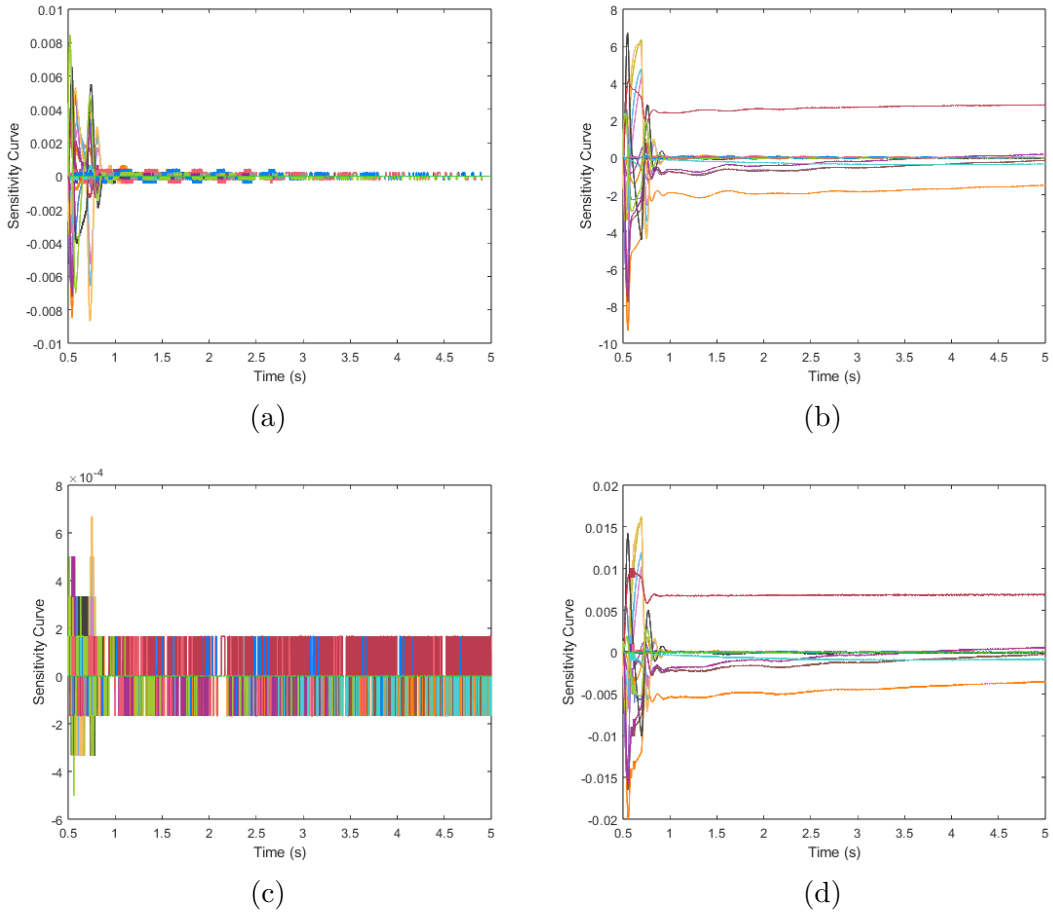

Source: Author

Based on the sensitivity results of the previous images, to study the frequency stability of the system, a smaller time window must be used. For the purpose of this study, the signal choosen to be the target for the estimatian is the Active Power (P). Thus, a closer look at its sensitivity analysis must be taken, the Figure 12 shows the zoomed version of sensitivity curves for the active power signal in Figure 11(a).

Figure 12 – Sensitivity Analysis of the Active Power signal from 0.500s to 1.0s

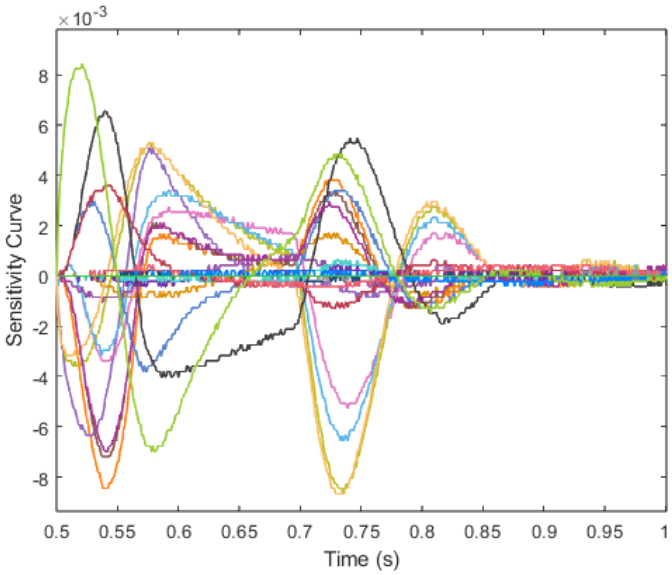

Source: Author

However, due to the large number of parameters, it is still difficult to differ the most sensitive ones in the image. In order to have a clear visualization, the next result in Figure 13 presents a filtered graph with the parameters with the highest sensitivity, and tags for the top 5 parameters:

Figure 13 – Active Power sensitivity analysis.

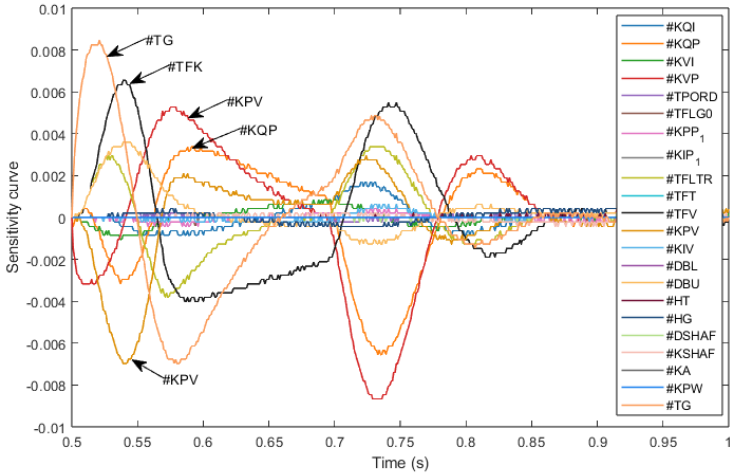

Source: Author

Similar to the analysis presented in Section 4.1.1, but now focusing on a refined time window from $T_1 = 0.500$s to 1.0s, and filtered to include only parameters with non-null values, Table 2 presents the sensitivity results for this busbars P and Q signals .

Table 2 – Filtered sensitivity indices of the 56532 busbar from 0.5s to 1.0s.

Control Block	θ_i	$E_{\theta_i}^{\hat{P}_T}$	$E_{\theta_i}^{\hat{Q}_T}$
reec_a	#KQI	0,00017	225,453
	#KQP	0,00272	2468,773
	#KVI	$7.662 \times 10{-}5$	100,517
	#KVP	0,00484	5247,650
	#TPORD	$9{,}159\times 10{-}6$	0,2590
	#TFLG0	$1{,}671\times 10{-}6$	0,7681
wtgtrq_a	#KPP_1	$1{,}653\times 10{-}5$	0,7586
	#KIP_1	$1{,}340\times 10{-}7$	0,0013
repca_a	#TFLTR	0,00112	962,739
	#TFV	0,00367	2867,627
	#KPV	0,00185	3084,667
	#KIV	$1{,}706\times 10{-}5$	20,649
	#DBU	0,00054	4020,635
wtgar_a	#HT	$2{,}457\times 10{-}6$	0,0366
	#HG	$3{,}721\times 10{-}5$	1,7961
	#DSHAF	$1{,}563\times 10{-}6$	0,0130
	#KSHAF	$1{,}25\times 10{-}5$	0,5970
regc_a	#TG	0,00496	1079,759

From Table 2, it is observed that in time window T_1, the most relevant parameters are TG, DBU, KPV, TFV, $TFLTR$, KVP, and KQP. These parameters are distributed across three different control blocks, each playing a specific role in the wind turbine operation. Outlined below are the definitions for each parameter and their respective control block:

- **P/Q control block (reec_a)**:
  - KVP: Represents the proportional gain of the active power control.
  - KQP: Defines the proportional gain of the reactive power control.
- **Plant level control model (repc_a)**:
  - TFV: Lag time constant.
  - TFLTR: Defines the voltage or reactive power measurement filter time constant.
  - KPV: Represents the proportional gain of the voltage control.
  - DBU: Defines the dead band used in reactive power control.
- **Generator/Converter module (regc_a)**:
  - TG: Represents the inverter current regulator lag time constant.

Considering the influence of parameters on both output signals, the parameter vector $\theta_s = [TG, DBU, KPV, TFV, TFLTR, KVP, KQP]$ is selected for estimation process.

To further illustrate the impact of these selected parameters, the graphs in Figure 14 show the response of the four signals of the model when the parameter TG (the most sensible in the Active Power signal) has its typical value increased by 90%, while on the other hand, the response of the model when the parameter KQI (with a relativity low sensitivity in the Active Power signal) has the same increase in its typical value:

Figure 14 – Nominal system response compared to the system response to a disturbance of 90% of the TG and KQI parameter value.

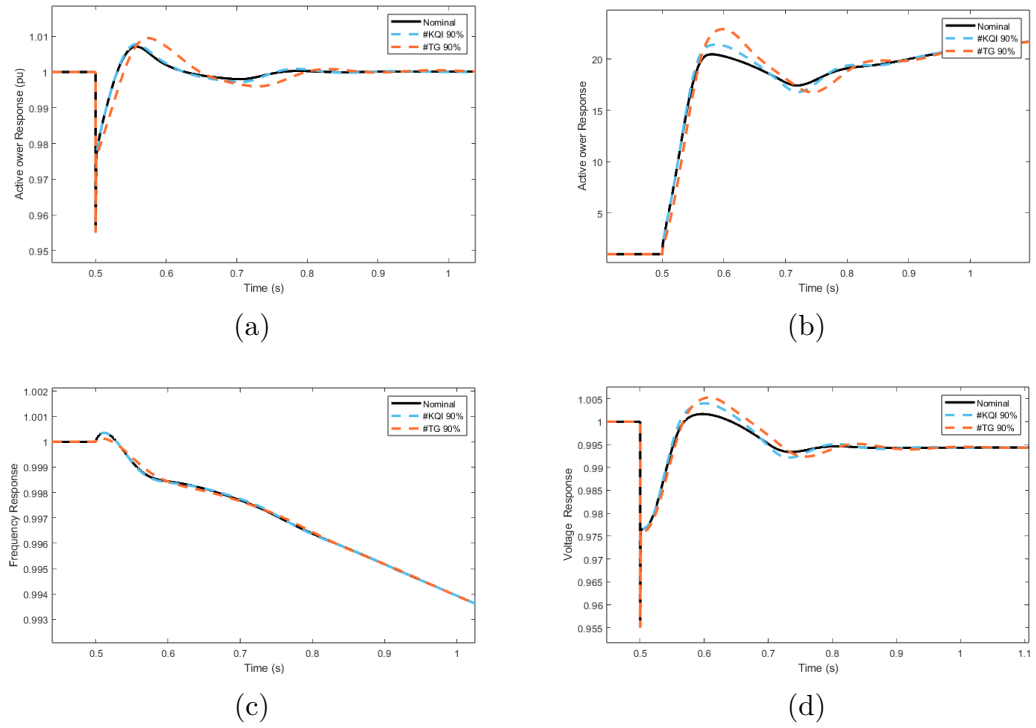

Source: Author

Although the figure above clearly shows a difference in the signal when the highest sensitivity parameter is modified (dashed orange curve), the overall impact remains moderate.

4.2 PARAMETER ESTIMATION

Given the results of the sensitivity analysis in the post-fault response period, the estimation is performed. For the application of the algorithm, the initial population of the DE consists of 15 individuals, with a mutation factor (F_s) of 0.6 and a crossover factor (C_r) of 0.3. The stopping criterion is met when the algorithm reaches 40 generations. The target aWF is the one connected to bus 53562, as mentioned previously.

The parameter vector (θ_s is estimated based on window $T_1 = 0.500$s to 0.650s, considering a search space of 40% relative to the initial values of each parameter. The remaining parameters are kept fixed at typical recommended values (ESIG, 2025).

The estimated values for each parameter are presented in Table 3. The comparison between the response of the aWF at bus 56532 (updated with the estimated parameters) and the reference system response at the same terminal bus is shown in Figure 15.

Table 3 – Parameters estimated by the proposed method for fitting the equivalent model.

	#KQP	**#KVP**	**#TFV**	**#KPV**	**#TG**
Estimated Values	0,60817 pu	1,3977 pu	0,2091 s	10,8115	0,01289 s
Typical Values	1 pu	1 pu	0.15 s	18	0.02 s

As observed, the active power response (Figure 15(a)) and frequency response (Figure 15(c)) are similar, providing a qualitative correspondence between the systems. Regarding reactive power (Figure 15(b) and voltage response (Figure 15(d)), the response provided by the WT3 model is slow and does not accurately capture the peaks observed in the manufacturer's model response at the fault application.

Figure 15 – (a) Active power, (b) Reactive power, (c) Frequency, (d) Voltage output by the adjusted WT3 model (connected to bar 56532) compared to the reference system.

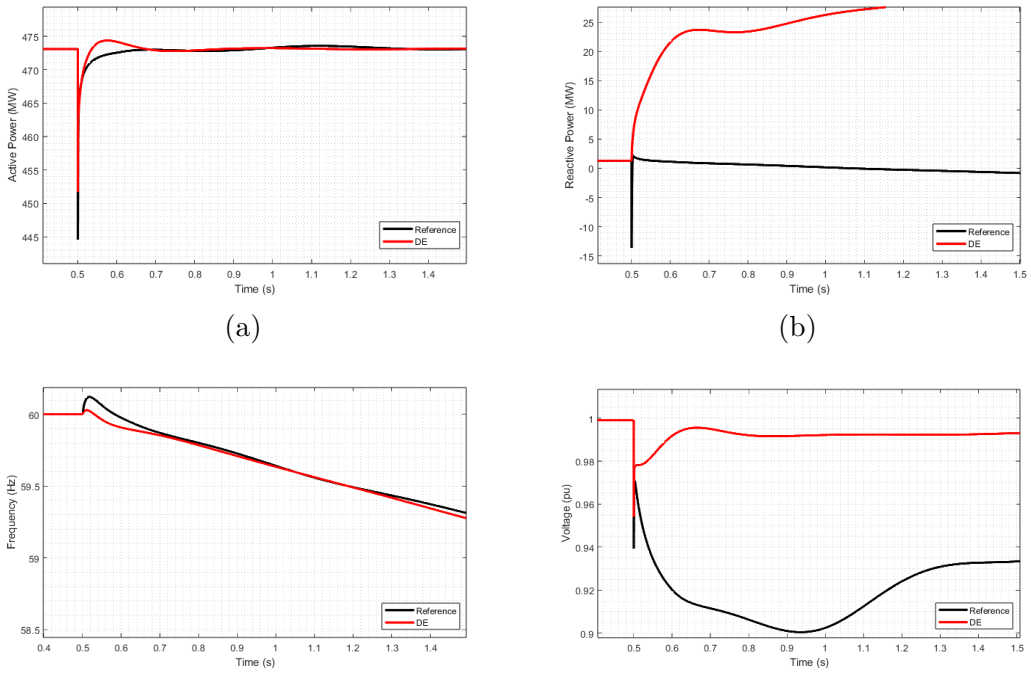

Source: Author.

5 CONCLUSION

The increasing penetration of wind energy in modern power systems has highlighted the importance of standardized models for frequency stability studies. In the Brazilian power system, ensuring a resilient grid requires validating mathematical models for wind power plants, making optimization methods essential to achieving this goal. Due to NDAs manufacturer-specific models are restricted, preventing system agents from directly simulating these proprietary models. As a result, one of the alternatives is to apply generic models to represent the dynamic behavior of WFs.

In conclusion, the primary contribution of this final thesis is the methodology that enables testing a model using the Sensitivity Analysis approach to approximate manufacturer models while reducing computational costs, ensuring it still represents the most relevant dynamics of selected model signals. The results presented reinforce the need for custom blocks in the generic models to accommodate the behavior of manufacturer models, as some discrepancies arise due to the specific procedures required by the Brazilian grid, which may not necessarily apply to a standardized international model.

One of the key advantages of generic models is their robustness and the reliability of the implemented structure. However, a major limitation is the simplification of the primary machine, which prevents the model from capturing certain behaviors associated with this component. Ideally, real-world measurements would be used for parameter estimation, but due to their unavailability, simulations are employed. Even if measurements were available, the lack of detail in the primary machine representation would still require additional modeling to reflect specific dynamics.

The TSA conducted in the Case Study of this research, applying the WT3 Phase II WECC, identified the parameters most sensitive to the disturbance of a sudden outage of the TPP Porto Sergipe are $TG, DBU, KPV, TFV, TFLTR, KVP$, and KQP. These parameters are distributed across three different control blocks: Generator/Converter module (regc_a); P/Q control block (reec_a); and Plant level control model (repc_a), and have the greatest impact on system response. Regarding parameterization, the results indicate that only the active power and frequency responses provide a qualitative correspondence between the generic and the manufacturers' reference model. Therefore, the work is suitable for applications in frequency stability studies.

A significant limitation observed is the significant discrepancy in reactive power response, which is primarily due to the discharge of the magnetic field under disturbance conditions. This phenomenon affects the accuracy of the WT3 model when replicating manufacturer models. Thus, if the primary objective is to evaluate active power or frequency dynamics, the WT3 model can be recommended. However, if the analysis requires an accurate representation of voltage and reactive power dynamics, modifications must be made to the model to improve its performance in these aspects.

One of the main challenges identified is achieving a more robust parameterization that reflects a wide range of scenarios. This would require the inclusion of multiple disturbances and operating conditions, as nonlinear systems can shift the sensitivity domain of parameters depending on the base case. Parameters of different natures may influence the system in very distinct ways depending on the operating point, which complicates the generalization of results.

Another important methodological consideration for future work is the composition of the objective function. In this study, the function was based on the combined error of active and reactive power signals. However, due to the difference in magnitude between these signals, the active power error dominates the optimization process, leading the algorithm to converge primarily toward minimizing active power discrepancies. A potential improvement would be to introduce weighting factors for each signal, allowing reactive power to contribute more significantly to the sensitivity analysis and parameter estimation.

Although this study focused primarily on the WT3 Phase II WECC, future research should explore alternative model versions or incorporate additional blocks to better represent specific transient dynamics of WF. However, adding new blocks depends on the completion of the ongoing update process coordinated by the ONS regarding manufacturer models. Other promising direction would be for manufacturers themselves to apply the proposed methodology to adapt generic models to their equipment. This would result in more reliable and clearly structured models that preserve essential dynamic responses while maintaining confidentiality and model integrity. Thus, refining and evolving these models is a promising direction for future research.

REFERENCES

ABEEÓLICA. **Associação Brasileira de Energia Eólica**. [S.l.: s.n.], 2022.

ALAM, M. S. et al. Solar and wind energy integrated system frequency control: a critical review on recent developments. **Energies**, Basel, v. 16, n. 2, 2023.

EIRÓ, Diogo. **WT3 Generic Models for Transient Stability Studies of Wind Turbine Generators**. [S.l.: s.n.], 2018.

EPE. **Empresa de Pesquisas Energéticas – Plano Decenal de Expansão de Energia Metodologia, versão PDE 2032**. [S.l.: s.n.], 2022.

ESIG. **Type 3 – Generic Wind Turbine Generator Model (Phase II)**. [S.l.: s.n.], 2025. Available from: https://www.esig.energy/wiki-main-page/type-3-generic-wind-turbine-generator-model-phase-ii/.

GERALDI, E. L.; FERNANDES, T. C. C.; PIARDI, A. B.; GRILO, A. P.; RAMOS, R. A. Parameter estimation of a synchronous generator model under unbalanced operating conditions. **Electric Power Systems Research**, v. 187, 2020.

HURTADO, M.; JAFARIAN, M.; KËRÇI, T.; TWEED, S.; ESCUDERO, M. V.; KENNEDY, E.; MILANO, F. Stability assessment of low-inertia power systems: a system operator perspective. In: IEEE Power & Energy Society General Meeting (PESGM). Seattle, WA, USA: IEEE, 2024. P. 1–5.

KUIAVA, Roman; RAMOS, Rodrigo; PAVANI, Ahda; BARBOSA, João Pedro; NASCIMENTO, Matheus; FERNANDES, Tatiane; FUCHS, Kamile. **Sistema de referência do subsistema Nordeste – lacsep-ne224**. [S.l.: s.n.], 2025. Available from: https://lacsep.github.io/lacsep-ne224.

KUNDUR, P. **Power System Stability and Control**. [S.l.]: McGraw-Hill Education, 1994. (EPRI Power System Engineering Series). ISBN 9780070359581.

LAMPINEN, K. V. P. M. S. J. A. **Differential Evolution: A Practical Approach to Global Optimization**. Berlin, Heidelberg: Springer, 2005.

LORENZO-BONACHE, A.; HONRUBIA-ESCRIBANO, A.; FORTMANN, J.; GÓMEZ-LÁZARO, E. Generic Type 3 WT Models: Comparison Between IEC and WECC Approaches. **IET Renewable Power Generation**, v. 13, p. 1168–1178, 2019.

ONS. **Base de dados de transitórios eletromecânicos para o programa ANATEM**. Rio de Janeiro, Brazil, Nov. 2024.

ONS. **RELATÓRIO DE ANÁLISE DE PERTURBAÇÃO - RAP 2023.08.15**. 2023. Available from: https://www.ons.org.br/AcervoDigitalDocumentosEPublicacoes/RAP%202023.08.15%2008h030min%20vers%C3%A3o%20final.pdf.

RAMOS, R. R.; GRILO-PAVANI, A. P.; PIARDI, A. B.; FERNANDES, T. C. C. Method to build equivalent models of microgrids for rms dynamic simulation of power systems. In: 11TH Bulk Power Systems Dynamics and Control Symposium (IREP). Banff, Canada: [s.n.], 2022.

WANG, P.; ZHANG, Z.; MA, T.; HUANG, Q.; LEE, W.-J. Parameter calibration of wind farm with error tracing technique and correlated parameter identification. **IEEE Transactions on Power Systems**, v. 38, n. 6, p. 5200–5214, Nov. 2023.

APPENDIX A – Typical Values - WT3 WECC

The WT3 modeling package includes 7 models: generator/converter model (regc_a), P/Q control (reec_a), plant level control (repc_a), torque control (wtgtra_a), pitch control (wtgpt_a), aero dynamic model (wtgar_a) and drive-train model (wtft_a). The block diagram of each of these models are shown in the (ESIG, 2025). The parameters values adopted in this report are shown in the following Tables 4 until 9.

Table 4 – Data for the plant level control model (repc_a).

Parameters			
Description	**Symbol**	**Unit**	**Value**
Voltage or reactive power measurement filter time constant	Tfltr	s	0.02
Lead time constant	Tft	s	0.02
Lag time constant	Tfv	s	0.4
Proportional gain	Kp	pu/pu	0.9
Integral gain	Ki	pu/pu	-1.3
Deadband downside	Dbl1	pu	1.2
Deadband upside	Dbl2	pu	1.5
Flag to turn on (1) or off (0) the active power control loop within the plant controller	Freq_flag		999.9
Selection of droop (0) or line drop compensation (1)	Vcompflag		-999.9
Minimum Q control output	Qmin	pu	10.0
Maximum Q control output	Qmax	pu	0.05
Maximum error limit	Emax	pu	0.2
Minimum error limit	Emin	pu	

Table 5 – Data for the drive-train model (wtgt_a) and aero-dynamic model (wtgar_a).

Parameters			
Description	**Symbol**	**Unit**	**Value**
Turbine inertia	Ht	MWs/MVA	3.96305
Generator inertia	Hg	MWs/MVA	0.72695
Damping coefficient	Dshaft	pu	1.5
Spring constant	Kshaft	pu	160
Aero-dynamic gain factor	Ka	pu/degrees	0.007
Initial pitch angle	\$\theta\$_a	degrees	0

Table 6 – Data for the P/Q control model (reec_a).

Parameters

Description	Symbol	Unit	Value
Filter time constant for electrical power measurement	Tp	s	0.01
Integral gain	Kqi	pu	3.0
Proportional gain	Kqp	pu	0.5
Integral gain	Kvi	pu	15.0
Proportional gain	Kvp	pu	4.5
Time constant on lag delay	Tiq	s	0.02
High voltage clamp logic acceleration factor	Khv	–	1.5
Filter time constant for electrical power measurement	Tp	s	0.05
The voltage below which the reactive current injection (Iqinj) logic is activated	Vdip	pu	0.85
The voltage above which the reactive current injection (Iqinj) logic is activated	Vup	pu	1.20
Filter time constant for voltage measurement	Trv	s	0.01
Deadband in voltage error when voltage dip logic is activated	dbd1	pu	0.05
Deadband in voltage error when voltage dip logic is activated (for undervoltage)	dbd2	pu	0.05
Gain for reactive current injection during voltage dip (and overvoltage) conditions	Kqv	pu/pu	0.8
Maximum limit of reactive current injection (Iqinj)	Iqh1	pu	0.75
Minimum limit of reactive current injection (Iqinj)	Iql1	pu	-0.75
			(Vq, Iq)
			(0.0, 0.75)
VDL1 Curve			(0.2, 0.750001)
			(0.5, 0.750002)
			(1.0, 0.750003)
			(Vp, Ip)
			(0.2, 1.11)
VDL2 Curve			(0.5, 1.110001)
			(0.75, 1.110002)
			(1.0, 1.110003)

Table 7 – Data for the torque controller model (wtgtrq_a).

Parameters			
Description	**Symbol**	**Unit**	**Value**
Power measurement lag time constant	Tp	s	0.05
Speed reference time constant	Twref	s	30.0
Proportional gain	Kpp	pu/pu	3.0
Integral gain	Kip	pu/pu	0.6
Maximum torque	Temax	pu	1.2
Minimum torque	Temin	pu	0.0
			(P, speed)
			(0.0, 0.7999)
P x speed curve			(0.04, 0.800)
			(0.2, 1.000)
			(1.0, 1.0001)

Table 8 – Data for the pitch controller model (wtgpt_a).

Parameters			
Description	**Symbol**	**Unit**	**Value**
Pitch-control proportional gain	Kpw	pu/pu	150.0
Pitch-control integral gain	Kiw	pu/pu	25.0
Proportional gain	Kcc	pu/pu	0.0
Pitch-compensation integral gain	Kic	pu/pu	30.0
Pitch time constant	Tth	s	0.3
Pitch-compensation proportional gain	Kpc	pu/pu	3.0
Maximum pitch angle	$d\theta$max	degrees	27.0
Minimum pitch angle	$d\theta$min	degrees	0.0
Maximum pitch angle rate	$d\theta$max	degrees/s	10.0
Minimum pitch angle rate	$d\theta$min	degrees/s	-10.0

Table 9 – Data for the generator/converter model (regc_a).

Parameters

Description	Symbol	Unit	Value
Inverter current regulator lag time constant	Tg	s	0.02
Terminal voltage filter (for LVPL) time constant	Tfltr	s	0.02
LVPL zero crossing	Zerox	pu	0.4
LVPL breakpoint	Brkpt	pu	0.9
Current limit for high voltage clamp logic	Iolim	pu	-1.3
Voltage limit for high voltage clamp logic	Volim	pu	1.2
High voltage clamp logic acceleration factor	Khv	–	1.5
Maximum rate-of-change of reactive current	Iqrmax	pu/s	999.9
Minimum rate-of-change of reactive current	Iqrmin	pu/s	-999.9
Active current up-ramp rate limit on voltage recovery	rrpwr	pu/s	10.0
Low voltage active current management breakpoint	lvpnt0	pu	0.05
Low voltage active current management breakpoint	Lvpnt1	pu	0.2

APPENDIX B – Sensitivity Analysis - RN busbars

The following Tables present the results of the ensitivity analysis performed on the Voltage (V), Frequency(F), Active Power (P) and Reactive Power (Q) sigals for the 76 parameters of the busbars in the RN region described in Table 1.

Busbar	Perubation	Time Step	Inicial Time (s)	Final time (s)
56311	0.01	0.1	0.5	5
θ_i	$E_{\theta_i}^{\hat{V}_T}$	$E_{\theta_i}^{\hat{P}_T}$	$E_{\theta_i}^{\hat{P}_T}$	$E_{\theta_i}^{\hat{Q}_T}$
#FLG_Q	0	0	0	0
#FLG_V	0	0	0	0
#FLG_F	0	0	0	0
#MBASE	0	0	0	0
#NMAQ	0	0	0	0
#PFLG0	0	0	0	0
#VFLG1	0	0	0	0
#VFLG0	0	0	0	0
#QFLG1	0	0	0	0
#QFLG0	0	0	0	0
#TP_1	0	0	0	0
#KQI	0.005881412	4.02778E-06	9.22698E-05	38.48356458
#KQP	0.009519469	7.44444E-06	0.000228137	64.35039688
#KVI	0.000296641	1.30556E-06	2.74597E-05	1.982415188
#KVP	0.000476231	1.66667E-06	0.000168532	3.663891792
#TIQ	0	0	0	0
#TPORD	3.20001E-06	7.5E-07	9.29205E-05	0.000609606
#VDIP	0	0	0	0
#VFRZ	0	0	0	0
#VUP	0	0	0	0
#TRV	0	0	0	0
#DBD1	0	0	0	0
#DBD2	0	0	0	0
#KQV	0	0	0	0
#IQH1	0	0	0	0
#IQL1	0	0	0	0
#TP	0	0	0	0
#TWREF	0	0	0	0
#TFLG1	0	0	0	0
#TFLG0	9.05002E-06	1.30556E-06	0.000235295	0.001822111
#KPP_1	9.04002E-06	1.25E-06	0.000235815	0.00183143
#KIP_1	2.48E-06	2.77778E-08	5.19262E-05	9.8664E-06
#TFLTR	0.000382101	1.61111E-06	4.77617E-05	2.631853612
#TFT	0	0	0	0
#TFV	0.003859228	5.27778E-06	0.000108928	25.93660635
#KPV	0.001258443	2.08333E-06	7.93859E-05	8.579261917
#KIV	0.001190192	2.72222E-06	5.20563E-06	8.241593292
#DBL	0.009649249	7.33333E-06	0.000246877	66.14769094
#DBU	0	0	0	0
#HT	7.02001E-06	6.66667E-07	0.000175039	0.000952788
#HG	3.69501E-05	5.58333E-06	0.002263409	0.035822644
#DSHAF	3.42001E-06	6.11111E-07	0.000102551	0.0004954
#KSHAF	3.75001E-05	6.13889E-06	0.002433764	0.038504367
#KA	1E-08	0	6.50704E-07	9.38168E-08
#KPW	2E-08	0	9.10986E-07	1.09453E-07
#KIW	0	0	3.90422E-07	3.12723E-08
#KCC	0	0	0	0
#KIC	0	0	0	0
#TTH	0	0	0	3.127E-08
#KPC	0	0	0	0
#PMX	0	0	0	0
#IMAX	0	0	0	0
#PQPRI	0	0	0	0
#VQ1	0	0	0	0
#IQ1	0	0	0	0
#VQ2	0	0	0	0
#IQ2	0	0	0	0
#VQ3	0	0	0	0
#IQ3	0	0	0	0
#VQ4	0	0	0	0
#IQ4	0	0	0	0
#VP1	0	0	0	0
#IP1	0	0	0	0
#VP2	0	0	0	0
#IP2	0	0	0	0
#VP3	0	0	0	0
#IP3	0	0	0	0
#VP4	0	0	0	0
#IP4	0	0	0	0
#TG	0.000525481	4.25E-06	0.002941052	3.531045531
#TFTR	0	0	0	0
#KHV	0	0	0	0
#IOLIM	0	0	0	0
#VOLIM	0	0	0	0
#LVPT1	0	0	0	0
#LVPT0	0	0	0	0

Busbar	Perubation	Time Step	Inicial Time (s)	Final time (s)
56477	0.01	0.1	0.5	5
θ_i	$E_{\theta_i}^{\hat{V}_T}$	$E_{\theta_i}^{\hat{P}_T}$	$E_{\theta_i}^{\hat{P}_T}$	$E_{\theta_i}^{\hat{Q}_T}$
#FLG_Q	0	0	0	0
#FLG_V	0	0	0	0
#FLG_F	0	0	0	0
#MBASE	0	0	0	0
#NMAQ	0	0	0	0
#PFLG0	0	0	0	0
#VFLG1	0	0	0	0
#VFLG0	0	0	0	0
#QFLG1	0	0	0	0
#QFLG0	0	0	0	0
#TP_1	0	0	0	0
#KQI	0.220834152	3.49722E-05	0.000688457	4214.071481
#KQP	0.140579701	3.61389E-05	0.001357416	2992.637123
#KVI	0.001467263	3.36111E-06	4.09268E-05	34.05367124
#KVP	0.007306685	9.22222E-06	0.00057598	239.4047162
#TIQ	0	0	0	0
#TPORD	6.11901E-05	3.55556E-06	0.000150864	1.834847661
#VDIP	0	0	0	0
#VFRZ	0	0	0	0
#VUP	0	0	0	0
#TRV	0	0	0	0
#DBD1	0	0	0	0
#DBD2	0	0	0	0
#KQV	0	0	0	0
#IQH1	0	0	0	0
#IQL1	0	0	0	0
#TP	0	0	0	0
#TWREF	0	0	0	0
#TFLG1	0	0	0	0
#TFLG0	0.000863792	6.94444E-06	0.000725699	6.167974938
#KPP_1	0.000850252	6.77778E-06	0.000683913	6.195631402
#KIP_1	7.22301E-05	3.61111E-07	6.57547E-05	0.024767482
#TFLTR	0.005636031	7.61111E-06	0.00020145	151.3584841
#TFT	0	0	0	0
#TFV	0.113610427	3.025E-05	0.001045994	2347.445972
#KPV	0.01493075	1.34444E-05	0.000522138	427.2618006
#KIV	0.015963072	1.06111E-05	9.95622E-05	373.5744692
#DBL	0.060998092	2.23611E-05	0.000704913	1568.856438
#DBU	0.173434057	4.38889E-05	0.00151565	3820.441881
#HT	0.000686331	4.88889E-06	0.000509259	4.669093661
#HG	0.006411323	3.89167E-05	0.010705998	193.1175312
#DSHAF	9.50802E-05	4.25E-06	0.000174762	2.621965303
#KSHAF	0.006818504	3.76667E-05	0.011507397	207.4077174
#KA	1.33E-06	2.77778E-08	1.39523E-06	2.52159E-05
#KPW	1.49E-06	2.77778E-08	1.68143E-06	3.37421E-05
#KIW	2.90001E-07	0	4.29302E-07	2.79301E-06
#KCC	0	0	0	0
#KIC	0	0	0	0
#TTH	1.4E-07	0	1.78876E-07	1.03969E-05
#KPC	0	0	0	0
#PMX	0	0	0	0
#IMAX	0	0	0	0
#PQPRI	0	0	0	0
#VQ1	0	0	0	0
#IQ1	0	0	0	0
#VQ2	0	0	0	0
#IQ2	0	0	0	0
#VQ3	0	0	0	0
#IQ3	0	0	0	0
#VQ4	0	0	0	0
#IQ4	0	0	0	0
#VP1	0	0	0	0
#IP1	0	0	0	0
#VP2	0	0	0	0
#IP2	0	0	0	0
#VP3	0	0	0	0
#IP3	0	0	0	0
#VP4	0	0	0	0
#IP4	0	0	0	0
#TG	0.013913738	2.35278E-05	0.008553229	88.62683397
#TFTR	0	0	0	0
#KHV	0	0	0	0
#IOLIM	0	0	0	0
#VOLIM	0	0	0	0
#LVPT1	0	0	0	0
#LVPT0	0	0	0	0

Busbar	Perubation	Time Step	Inicial Time (s)	Final time (s)
56515	0.01	0.1	0.5	5
θ_i	$E_{\theta_i}^{\hat{V}_T}$	$E_{\theta_i}^{\hat{P}_T}$	$E_{\theta_i}^{\hat{P}_T}$	$E_{\theta_i}^{\hat{Q}_T}$
#FLG_Q	0	0	0	0
#FLG_V	0	0	0	0
#FLG_F	0	0	0	0
#MBASE	0	0	0	0
#NMAQ	0	0	0	0
#PFLG0	0	0	0	0
#VFLG1	0	0	0	0
#VFLG0	0	0	0	0
#QFLG1	0	0	0	0
#QFLG0	0	0	0	0
#TP_1	0	0	0	0
#KQI	0.001677447	3.16667E-06	0.000231298	17.18430468
#KQP	0.0160171	1.925E-05	0.003632246	194.5036909
#KVI	0.000800512	2.41667E-06	0.00012319	7.900010204
#KVP	0.036930478	3.65278E-05	0.006790405	418.692744
#TIQ	0	0	0	0
#TPORD	9.36875E-06	6.38889E-07	2.3889E-05	0.038903911
#VDIP	0	0	0	0
#VFRZ	0	0	0	0
#VUP	0	0	0	0
#TRV	0	0	0	0
#DBD1	0	0	0	0
#DBD2	0	0	0	0
#KQV	0	0	0	0
#IQH1	0	0	0	0
#IQL1	0	0	0	0
#TP	0	0	0	0
#TWREF	0	0	0	0
#TFLG1	0	0	0	0
#TFLG0	6.82365E-06	7.22222E-07	4.46907E-05	0.11439522
#KPP_1	6.79359E-06	7.22222E-07	4.46907E-05	0.113275461
#KIP_1	7.01404E-08	5.55556E-08	4.30205E-06	0.002783987
#TFLTR	0.006115808	8.36111E-06	0.001337381	72.6365147
#TFT	0	0	0	0
#TFV	0.019614559	2.63333E-05	0.005302909	249.5421072
#KPV	0.017607873	1.35556E-05	0.001001264	155.5337327
#KIV	0.002995584	4.16667E-06	3.1329E-05	25.37230507
#DBL	0	0	0	0
#DBU	0.214937369	3.69722E-05	0.000431318	1822.314794
#HT	8.81764E-07	3.61111E-07	2.25225E-05	0.022348946
#HG	1.76553E-05	3.25E-06	0.000232311	0.953602975
#DSHAF	8.71744E-07	2.77778E-07	1.77649E-05	0.014510635
#KSHAF	5.93187E-06	2.61111E-06	0.000202348	0.817084866
#KA	0	0	0	5.13651E-06
#KPW	0	0	0	5.13651E-06
#KIW	0	0	0	0
#KCC	0	0	0	0
#KIC	0	0	0	0
#TTH	0	0	0	0
#KPC	0	0	0	0
#PMX	0	0	0	0
#IMAX	0	0	0	0
#PQPRI	0	0	0	0
#VQ1	0	0	0	0
#IQ1	0	0	0	0
#VQ2	0	0	0	0
#IQ2	0	0	0	0
#VQ3	0	0	0	0
#IQ3	0	0	0	0
#VQ4	0	0	0	0
#IQ4	0	0	0	0
#VP1	0	0	0	0
#IP1	0	0	0	0
#VP2	0	0	0	0
#IP2	0	0	0	0
#VP3	0	0	0	0
#IP3	0	0	0	0
#VP4	0	0	0	0
#IP4	0	0	0	0
#TG	0.003988361	1.97222E-05	0.00592291	83.46145989
#TFTR	0	0	0	0
#KHV	0	0	0	0
#IOLIM	0	0	0	0
#VOLIM	0	0	0	0
#LVPT1	0	0	0	0
#LVPT0	0	0	0	0

Busbar	Perubation	Time Step	Inicial Time (s)	Final time (s)
56691	0.01	0.1	0.5	5
θ_i	$E_{\theta_i}^{\hat{V}_T}$	$E_{\theta_i}^{\hat{P}_T}$	$E_{\theta_i}^{\hat{P}_T}$	$E_{\theta_i}^{\hat{Q}_T}$
#FLG_Q	0	0	0	0
#FLG_V	0	0	0	0
#FLG_F	0	0	0	0
#MBASE	0	0	0	0
#NMAQ	0	0	0	0
#PFLG0	0	0	0	0
#VFLG1	0	0	0	0
#VFLG0	0	0	0	0
#QFLG1	0	0	0	0
#QFLG0	0	0	0	0
#TP_1	0	0	0	0
#KQI	0.003220429	2.52778E-06	6.1144E-05	1.235145083
#KQP	0.004863505	4.5E-06	0.000137254	1.897389638
#KVI	0.000231545	1E-06	2.25133E-05	0.088164444
#KVP	0.000270822	8.88889E-07	0.000127277	0.117887968
#TIQ	0	0	0	0
#TPORD	2.21887E-06	6.11111E-07	7.6366E-05	3.95573E-05
#VDIP	0	0	0	0
#VFRZ	0	0	0	0
#VUP	0	0	0	0
#TRV	0	0	0	0
#DBD1	0	0	0	0
#DBD2	0	0	0	0
#KQV	0	0	0	0
#IQH1	0	0	0	0
#IQL1	0	0	0	0
#TP	0	0	0	0
#TWREF	0	0	0	0
#TFLG1	0	0	0	0
#TFLG0	5.93371E-06	7.22222E-07	0.000178571	7.51045E-05
#KPP_1	5.81323E-06	7.22222E-07	0.000178571	7.57163E-05
#KIP_1	1.71686E-06	5.55556E-08	4.23403E-05	3.12652E-06
#TFLTR	0.000191716	9.44444E-07	3.12116E-05	0.07363202
#TFT	0	0	0	0
#TFV	0.001738889	2.66667E-06	6.13998E-05	0.674184342
#KPV	0.00058315	1.47222E-06	4.46428E-05	0.2283291
#KIV	0.000546865	1.13889E-06	3.06999E-06	0.211703196
#DBL	0.007235533	5.36111E-06	0.000202236	2.855648256
#DBU	0	0	0	0
#HT	4.49797E-06	6.11111E-07	0.000139557	6.27344E-05
#HG	2.24397E-05	5.16667E-06	0.001578103	0.000822004
#DSHAF	2.22891E-06	5.55556E-07	9.13322E-05	4.36354E-05
#KSHAF	2.29618E-05	4.25E-06	0.001680308	0.000879437
#KA	2.00802E-08	0	1.27916E-07	6.79679E-08
#KPW	2.00802E-08	0	1.27916E-07	1.35936E-07
#KIW	1.00401E-08	0	0	6.79679E-08
#KCC	0	0	0	0
#KIC	0	0	0	0
#TTH	0	0	0	0
#KPC	0	0	0	0
#PMX	0	0	0	0
#IMAX	0	0	0	0
#PQPRI	0	0	0	0
#VQ1	0	0	0	0
#IQ1	0	0	0	0
#VQ2	0	0	0	0
#IQ2	0	0	0	0
#VQ3	0	0	0	0
#IQ3	0	0	0	0
#VQ4	0	0	0	0
#IQ4	0	0	0	0
#VP1	0	0	0	0
#IP1	0	0	0	0
#VP2	0	0	0	0
#IP2	0	0	0	0
#VP3	0	0	0	0
#IP3	0	0	0	0
#VP4	0	0	0	0
#IP4	0	0	0	0
#TG	0.000333593	2.41667E-06	0.00219517	0.131030856
#TFTR	0	0	0	0
#KHV	0	0	0	0
#IOLIM	0	0	0	0
#VOLIM	0	0	0	0
#LVPT1	0	0	0	0
#LVPT0	0	0	0	0

Busbar	Perubation	Time Step	Inicial Time (s)	Final time (s)
56720	0.01	0.1	0.5	5
θ_i	$E_{\theta_i}^{\hat{v}_T}$	$E_{\theta_i}^{\hat{P}_T}$	$E_{\theta_i}^{\hat{\theta}_T}$	$E_{\theta_i}^{\hat{Q}_T}$
#FLG_Q	0	0	0	0
#FLG_V	0	0	0	0
#FLG_F	0	0	0	0
#MBASE	0	0	0	0
#NMAQ	0	0	0	0
#PFLG0	0	0	0	0
#VFLG1	0	0	0	0
#VFLG0	0	0	0	0
#QFLG1	0	0	0	0
#QFLG0	0	0	0	0
#TP_1	0	0	0	0
#KQI	0.000165853	1.66667E-07	7.29835E-05	7.486762642
#KQP	0.000517418	5.55556E-07	0.000182688	24.28204016
#KVI	0.000242379	1.94444E-07	8.859E-05	11.0144661
#KVP	0.000717567	7.5E-07	0.000222163	33.48006921
#TIQ	0	0	0	0
#TPORD	2.61043E-07	5.55556E-08	6.70163E-05	0.001679386
#VDIP	0	0	0	0
#VFRZ	0	0	0	0
#VUP	0	0	0	0
#TRV	0	0	0	0
#DBD1	0	0	0	0
#DBD2	0	0	0	0
#KQV	0	0	0	0
#IQH1	0	0	0	0
#IQL1	0	0	0	0
#TP	0	0	0	0
#TWREF	0	0	0	0
#TFLG1	0	0	0	0
#TFLG0	2.51003E-07	5.55556E-08	0.000129442	0.003472793
#KPP_1	2.30923E-07	5.55556E-08	0.000134492	0.003567495
#KIP_1	0	0	1.79016E-05	0.000429317
#TFLTR	0.000224266	2.77778E-07	9.45572E-05	10.31993972
#TFT	0	0	0	0
#TFV	0.002998542	1.47222E-06	0.000586622	139.2450588
#KPV	0.012688182	7.83333E-06	0.000669244	591.2041409
#KIV	0.005542377	3.97222E-06	2.29508E-05	263.0448772
#DBL	0	0	0	0
#DBU	0.180162479	3.24444E-05	0.000278163	8577.534808
#HT	2.10843E-07	1.38889E-07	9.59342E-05	0.002443317
#HG	1.59638E-06	8.33333E-07	0.000654097	0.019047768
#DSHAF	9.03611E-08	2.77778E-08	7.71146E-05	0.001849849
#KSHAF	1.23493E-06	8.05556E-07	0.000590753	0.018889931
#KA	0	0	0	0
#KPW	0	0	0	0
#KIW	0	0	0	0
#KCC	0	0	0	0
#KIC	0	0	0	0
#TTH	0	0	0	0
#KPC	0	0	0	0
#PMX	0	0	0	0
#IMAX	0	0	0	0
#PQPRI	0	0	0	0
#VQ1	0	0	0	0
#IQ1	0	0	0	0
#VQ2	0	0	0	0
#IQ2	0	0	0	0
#VQ3	0	0	0	0
#IQ3	0	0	0	0
#VQ4	0	0	0	0
#IQ4	0	0	0	0
#VP1	0	0	0	0
#IP1	0	0	0	0
#VP2	0	0	0	0
#IP2	0	0	0	0
#VP3	0	0	0	0
#IP3	0	0	0	0
#VP4	0	0	0	0
#IP4	0	0	0	0
#TG	0.000138985	9.16667E-07	0.001883799	7.675963796
#TFTR	0	0	0	0
#KHV	0	0	0	0
#IOLIM	0	0	0	0
#VOLIM	0	0	0	0
#LVPT1	0	0	0	0
#LVPT0	0	0	0	0

Busbar	Perubation	Time Step	Inicial Time (s)	Final time (s)
56749	0.01	0.1	0.5	5
θ_i	$E_{\theta_i}^{\hat{v}_T}$	$E_{\theta_i}^{\hat{P}_T}$	$E_{\theta_i}^{\hat{\theta}_T}$	$E_{\theta_i}^{\hat{Q}_T}$
#FLG_Q	0	0	0	0
#FLG_V	0	0	0	0
#FLG_F	0	0	0	0
#MBASE	0	0	0	0
#NMAQ	0	0	0	0
#PFLG0	0	0	0	0
#VFLG1	0	0	0	0
#VFLG0	0	0	0	0
#QFLG1	0	0	0	0
#QFLG0	0	0	0	0
#TP_1	0	0	0	0
#KQI	0.00048707	1.25E-06	2.49869E-05	1.032194374
#KQP	0.00133245	3.88889E-06	5.49152E-05	2.914077614
#KVI	4.642E-05	5E-07	1.02558E-05	0.087596628
#KVP	8.033E-05	3.88889E-07	3.27254E-05	0.169980415
#TIQ	0	0	0	0
#TPORD	4.4E-07	1.66667E-07	6.56372E-05	8.1966E-06
#VDIP	0	0	0	0
#VFRZ	0	0	0	0
#VUP	0	0	0	0
#TRV	0	0	0	0
#DBD1	0	0	0	0
#DBD2	0	0	0	0
#KQV	0	0	0	0
#IQH1	0	0	0	0
#IQL1	0	0	0	0
#TP	0	0	0	0
#TWREF	0	0	0	0
#TFLG1	0	0	0	0
#TFLG0	1.08E-06	3.61111E-07	0.000160457	1.41845E-05
#KPP_1	1.12E-06	2.77778E-07	0.000161109	1.39391E-05
#KIP_1	2.5E-07	0	3.10471E-05	4.90814E-07
#TFLTR	5.111E-05	6.66667E-07	9.6964E-06	0.094989569
#TFT	0	0	0	0
#TFV	0.00042177	2.22222E-06	2.59192E-05	0.912371461
#KPV	0.0001836	7.77778E-07	1.81808E-05	0.39096749
#KIV	0.0001322	1.66667E-06	1.67822E-06	0.282313255
#DBL	0.00112158	3.38889E-06	4.79226E-05	2.466503811
#DBU	0	0	0	0
#HT	1.03E-06	3.88889E-07	0.000118594	1.14851E-05
#HG	4.78E-06	1.55556E-06	0.001627597	7.75978E-05
#DSHAF	6.3E-07	1.94444E-07	7.49607E-05	8.09844E-06
#KSHAF	4.74E-06	1.38889E-06	0.001719154	7.70088E-05
#KA	1E-08	0	9.32347E-08	0
#KPW	1E-08	0	9.32347E-08	0
#KIW	0	0	0	0
#KCC	0	0	0	0
#KIC	0	0	0	0
#TTH	0	0	0	0
#KPC	0	0	0	0
#PMX	0	0	0	0
#IMAX	0	0	0	0
#PQPRI	0	0	0	0
#VQ1	0	0	0	0
#IQ1	0	0	0	0
#VQ2	0	0	0	0
#IQ2	0	0	0	0
#VQ3	0	0	0	0
#IQ3	0	0	0	0
#VQ4	0	0	0	0
#IQ4	0	0	0	0
#VP1	0	0	0	0
#IP1	0	0	0	0
#VP2	0	0	0	0
#IP2	0	0	0	0
#VP3	0	0	0	0
#IP3	0	0	0	0
#VP4	0	0	0	0
#IP4	0	0	0	0
#TG	9.591E-05	1.38889E-06	0.0022932	0.195808247
#TFTR	0	0	0	0
#KHV	0	0	0	0
#IOLIM	0	0	0	0
#VOLIM	0	0	0	0
#LVPT1	0	0	0	0
#LVPT0	0	0	0	0

Busbar	Perubation	Time Step	Inicial Time (s)	Final time (s)
56760	0.01	0.1	0.5	5
θ_i	$E_{\theta_i}^{\hat{v}_T}$	$E_{\theta_i}^{\hat{P}_T}$	$E_{\theta_i}^{\hat{\theta}_T}$	$E_{\theta_i}^{\hat{Q}_T}$
#FLG_Q	0	0	0	0
#FLG_V	0	0	0	0
#FLG_F	0	0	0	0
#MBASE	0	0	0	0
#NMAQ	0	0	0	0
#PFLG0	0	0	0	0
#VFLG1	0	0	0	0
#VFLG0	0	0	0	0
#QFLG1	0	0	0	0
#QFLG0	0	0	0	0
#TP_1	0	0	0	0
#KQI	0.000193624	2.22222E-07	6.51638E-05	2.255427066
#KQP	0.000432729	6.11111E-07	0.000124871	5.130505188
#KVI	0.000280862	2.77778E-07	7.7362E-05	3.257827436
#KVP	0.000602819	5.27778E-07	0.000152477	7.099204885
#TIQ	0	0	0	0
#TPORD	3.01204E-07	1.38889E-07	7.41519E-05	0.000233638
#VDIP	0	0	0	0
#VFRZ	0	0	0	0
#VUP	0	0	0	0
#TRV	0	0	0	0
#DBD1	0	0	0	0
#DBD2	0	0	0	0
#KQV	0	0	0	0
#IQH1	0	0	0	0
#IQL1	0	0	0	0
#TP	0	0	0	0
#TWREF	0	0	0	0
#TFLG1	0	0	0	0
#TFLG0	4.21685E-07	1.94444E-07	0.000147341	0.000483776
#KPP_1	4.21685E-07	1.94444E-07	0.000147983	0.000491036
#KIP_1	1.00401E-08	0	1.34822E-05	4.42196E-05
#TFLTR	0.000158925	2.5E-07	6.13118E-05	1.805741105
#TFT	0	0	0	0
#TFV	0.002977699	1.72222E-06	0.000426293	35.03456152
#KPV	0.018442988	1.675E-05	0.000497235	220.2277481
#KIV	0.009153367	9.16667E-06	1.50872E-05	112.2240093
#DBL	0	0	0	0
#DBU	0.164485645	4.83056E-05	0.000208332	2020.362926
#HT	3.11244E-07	1.94444E-07	0.000101437	0.000318777
#HG	1.98794E-06	1E-06	0.000723543	0.003037955
#DSHAF	2.20883E-07	5.55556E-08	6.80529E-05	0.000254098
#KSHAF	1.88754E-06	6.66667E-07	0.000755644	0.003105934
#KA	0	0	0	0
#KPW	0	0	0	0
#KIW	0	0	0	0
#KCC	0	0	0	0
#KIC	0	0	0	0
#TTH	0	0	0	0
#KPC	0	0	0	0
#PMX	0	0	0	0
#IMAX	0	0	0	0
#PQPRI	0	0	0	0
#VQ1	0	0	0	0
#IQ1	0	0	0	0
#VQ2	0	0	0	0
#IQ2	0	0	0	0
#VQ3	0	0	0	0
#IQ3	0	0	0	0
#VQ4	0	0	0	0
#IQ4	0	0	0	0
#VP1	0	0	0	0
#IP1	0	0	0	0
#VP2	0	0	0	0
#IP2	0	0	0	0
#VP3	0	0	0	0
#IP3	0	0	0	0
#VP4	0	0	0	0
#IP4	0	0	0	0
#TG	9.53912E-05	8.88889E-07	0.001928593	1.306114678
#TFTR	0	0	0	0
#KHV	0	0	0	0
#IOLIM	0	0	0	0
#VOLIM	0	0	0	0
#LVPT1	0	0	0	0
#LVPT0	0	0	0	0

Busbar	Perubation	Time Step	Inicial Time (s)	Final time (s)
56532	0.01	0.1	0.5	5
θ_i	$E_{\theta_i}^{\hat{v}_T}$	$E_{\theta_i}^{\hat{P}_T}$	$E_{\theta_i}^{\hat{\theta}_T}$	$E_{\theta_i}^{\hat{Q}_T}$
#FLG_Q	0	0	0	0
#FLG_V	0	0	0	0
#FLG_F	0	0	0	0
#MBASE	0	0	0	0
#NMAQ	0	0	0	0
#PFLG0	0	0	0	0
#VFLG1	0	0	0	0
#VFLG0	0	0	0	0
#QFLG1	0	0	0	0
#QFLG0	0	0	0	0
#TP_1	0	0	0	0
#KQI	0.001264761	3.19444E-06	0.000185548	226.2523813
#KQP	0.012053289	1.32222E-05	0.002760835	2470.771628
#KVI	0.000585952	1.94444E-06	8.69881E-05	101.1066249
#KVP	0.027537883	2.31944E-05	0.004923341	5254.110471
#TIQ	0	0	0	0
#TPORD	5.43087E-06	7.77778E-07	1.98817E-05	0.366513942
#VDIP	0	0	0	0
#VFRZ	0	0	0	0
#VUP	0	0	0	0
#TRV	0	0	0	0
#DBD1	0	0	0	0
#DBD2	0	0	0	0
#KQV	0	0	0	0
#IQH1	0	0	0	0
#IQL1	0	0	0	0
#TP	0	0	0	0
#TWREF	0	0	0	0
#TFLG1	0	0	0	0
#TFLG0	6.11223E-06	6.94444E-07	3.58765E-05	1.037305528
#KPP_1	6.16233E-06	6.94444E-07	3.67253E-05	1.02486061
#KIP_1	7.01404E-08	0	5.04862E-06	0.034192722
#TFLTR	0.004662249	6.77778E-06	0.001137994	963.6030416
#TFT	0	0	0	0
#TFV	0.013594543	1.63889E-05	0.003696035	2873.711352
#KPV	0.021639891	1.67222E-05	0.001903508	3545.532464
#KIV	0.002851305	3.94444E-06	2.22943E-05	435.6589148
#DBL	0	0	0	0
#DBU	0.214638571	4.04444E-05	0.000585952	33121.42092
#HT	6.71343E-07	3.33333E-07	1.88541E-05	0.212549352
#HG	9.36875E-06	2.38889E-06	0.000175317	7.978121878
#DSHAF	6.51303E-07	3.61111E-07	1.52352E-05	0.132458292
#KSHAF	4.92986E-06	1.97222E-06	0.000144936	6.751060297
#KA	0	0	0	6.16085E-05
#KPW	0	0	0	6.16085E-05
#KIW	0	0	0	0
#KCC	0	0	0	0
#KIC	0	0	0	0
#TTH	0	0	0	0
#KPC	0	0	0	0
#PMX	0	0	0	0
#IMAX	0	0	0	0
#PQPRI	0	0	0	0
#VQ1	0	0	0	0
#IQ1	0	0	0	0
#VQ2	0	0	0	0
#IQ2	0	0	0	0
#VQ3	0	0	0	0
#IQ3	0	0	0	0
#VQ4	0	0	0	0
#IQ4	0	0	0	0
#VP1	0	0	0	0
#IP1	0	0	0	0
#VP2	0	0	0	0
#IP2	0	0	0	0
#VP3	0	0	0	0
#IP3	0	0	0	0
#VP4	0	0	0	0
#IP4	0	0	0	0
#TG	0.003395514	1.29444E-05	0.004997685	1081.164918
#TFTR	0	0	0	0
#KHV	0	0	0	0
#IOLIM	0	0	0	0
#VOLIM	0	0	0	0
#LVPT1	0	0	0	0
#LVPT0	0	0	0	0